Review

Recent Developments in Rhodamine-Based Chemosensors: A Review of the Years 2018–2022

Yujiao Wang [ORCID], Xiaojun Wang, Wenyu Ma, Runhua Lu, Wenfeng Zhou and Haixiang Gao *

College of Science, China Agricultural University, Mingyuanxilu No.2, Haidian District, Beijing 100193, China
* Correspondence: hxgao@cau.edu.cn

Abstract: Chemosensors based on traditional fluorescent dyes have always contributed to the development of chemical sensor areas. In this review, the rhodamine-based chemosensors' improvements and applications from 2018 to 2022 are discussed, mainly focusing on cations (metal ions and H^+), anions (CN^-, F^-, etc.), and small bio-functional molecules' (thiols, amino acids, etc.) detection. Specifically, this review highlights the detection target, detection limit, detection solution system, detection mechanism, and performance of the rhodamine-based sensors. Although these rhodamine-based sensors are well developed, their repeatability and sensitivity still need significant improvement. This review is expected to bring new clues and bright ideas to researchers for further advances in rhodamine-based chemosensors in the future.

Keywords: chemosensor; rhodamine

1. Introduction

Chemosensors, since their first exploitation in 1864, have since then been playing a vital role in analytical chemistry due to their high sensitivity, time efficiency, simple operation, and less complicated instruments [1–5]. These sensors have been useful in identifying targets such as cations (H^+ and metal ions), anions (CN^-, F^-, etc.), and biomolecules (NADH, ATP, etc.) [6–8]. The detection of those targets is of great significance for monitoring food safety and human health. According to the Chinese standard, the threshold limit values in drinking water of Hg^{2+}, Pb^{2+}, As^{3+}, CN^-, F^- are 0.001, 0.01, 0.01, 1.5, 0.01 mg/L (5.0×10^{-9}, 4.8×10^{-8}, 4.8×10^{-7}, 7.9×10^{-5}, 3.8×10^{-7} M), respectively [9]. Traditional organic dyes contain a fluorescent core skeleton with a large conjugate system and auxochrome group altering wavelengths and enhancing fluorescence (such as amino, amide, etc.). In addition, many kinds of fluorescent materials have been developed, such as gold nanoparticles [10], quantum dots [11], metal-organic frameworks [12] covalent organic frameworks [13], and so on, as the development in fluorescent detection technology continues [14]. Although these emerging materials are widely used as fluorescent probes, cheap and easily synthetic organic dyes, such as rhodamine and its derivatives, are not replaced because of their great characteristics of convenience for structural modification, excellent molecular stability, and gratifying environmental compatibility [6].

Rhodamine, a group of xanthene-derivative dyes (Figure 1A) [15], was first prepared in 1905 by Noelting and Dziewonsky [16] and used for analytical research purposes (colorimetric detection of zinc, silver, etc.) from the middle of the 20th century [17]. Since Czarnik et al. [18] and Tae et al. [19], who pioneered works on rhodamine B and rhodamine 6G derivatives, respectively, as the fluorescent chemosensors for metal ions (Cu^{2+} and Hg^{2+}), a lot of sophisticated researches on rhodamine have been published, among which rhodamine B-based and rhodamine 6G-based chemosensors were those most often referred. As displayed in Figure 1B, the unique and convenient close-open ring structure of rhodamine derivatives before and after the addition target would induce color and fluorescent changes, helping greatly to detect target analyte. The coordination between the sensor and

target ion induces spirolactam ring opening and pronounces the colorimetric and/or fluorescent responses, which are usually non-fluorescent and colorless before the coordination (Figure 1B). Additionally, the rhodamine derivatives' properties of fine biocompatibility and near-infrared fluorescence make them an excellent choice for bio-sensor construction.
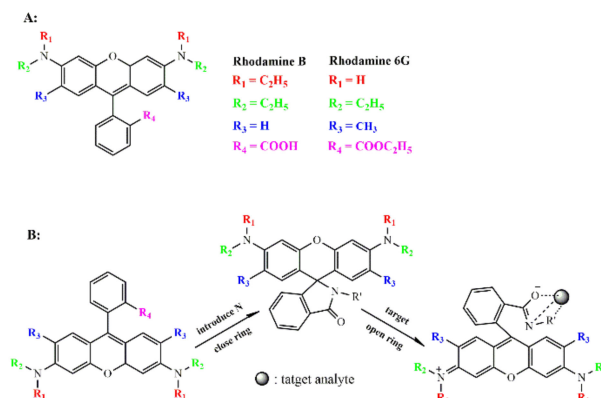

Figure 1. Chemical structures of rhodamine B and rhodamine 6G (**A**) and the general sensing principles of rhodamine-based sensors (**B**).

Many reviews on chemosensors research have been reported in the last two decades. Chen et al. described and discussed mercury-ion sensors from 2008 to 2015 [20]. Kaur et al. comprehensively summarized the developments of colorimetric sensors for metal ions from 2011–2016 [1]. Roy, P. discussed recently reported sensors for aluminum detection [21]. These reviews mainly focused on chemosensor targets. Chen et al. described the progress of benzazole-based fluorescent probes, reported in 2017–2019, combining the design strategy, synthetic route, sensing mechanism, and applications [6]. Jain, N. and Kaur, N. published a review on chemosensors based on 1,8-naphthalimide reported during 2017–2021 [22]. Zhu, H., et al. reviewed the advances of 4-hydroxy-1,8-naphthalimide-based chemosensors in the past decade [23]. These reviews elaborated on the chromophores of chemosensors.

However, as a classic chromophore for chemosensor construction, there are no reviews on the developments of rhodamine-based chemosensors in recent years. The sensing mechanism of rhodamine-based sensors has been proposed to guide the sensor's design [24]. The most common sensing mechanisms are photoinduced electron transfer (PET) [25,26], intramolecular charge transfer (ICT) [27,28], and fluorescence-resonance energy transfer (FRET) [24,29]. In this review, the endeavors of chemosensors based on rhodamine and its derivative from 2018 to 2022 are summarized and discussed. Generally, the colorless and non-fluorescent rhodamine turns red and shows a strong fluorescence when its closed spiro-ring is opened by metal complexation, analyte binding, or exposure to acidic conditions [17,30]. The rhodamine-based chemosensors are divided into three main categories according to the chemo sensor's targets: cations (metal ions, H^+), anions (CN^-, F^-, etc.), and small bio-functional molecules (H_2O_2, ATP, NADH). The concrete progress in this research area is elaborated in following sections. This review could bring new clues or bright ideas for further advances in rhodamine-based chemosensors in the future.

2. Rhodamine-Based Sensors for Metal Ions

Metal ions are partly beneficial to the body up to a certain concentration level. For example, iron (III), zinc (II), and copper (II) play vital roles in neurophysiology and neuropathology [31], however, their alleviated levels are harmful and may cause physiological disorders [32]. Other metals, such as mercury (II), lead (II), cadmium (III), and chromium (III) are potentially toxic to both humans and the environment [1,5]. Hence, monitoring the levels of these metal ions in living bodies and the environments (groundwater, industrial sewage, and so on) is quite significant. Table 1 shows the reported fluorescent probes based on rhodamine derivatives, generally designed for divalent (Hg^{2+}, Cu^{2+}, Pb^{2+}, Zn^{2+}, Cd^{2+}, Co^{2+}) and trivalent (Fes^{3+}, Cr^{3+}, Al^{3+}, As^{3+}) metal ions.

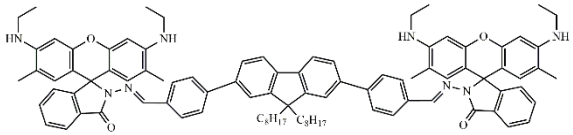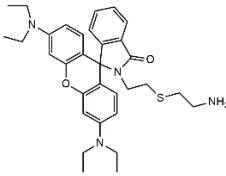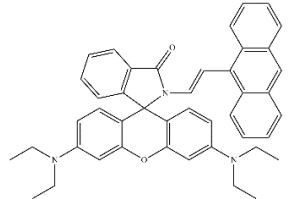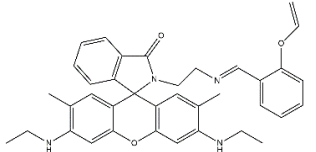**Table 1.** Rhodamine-based sensors for metal ions.

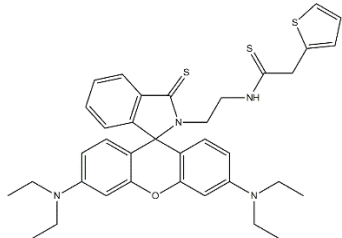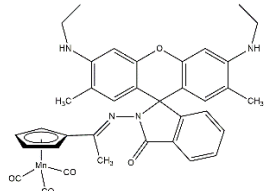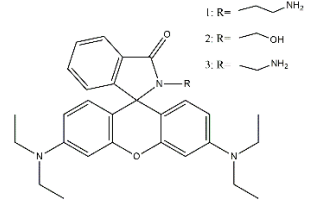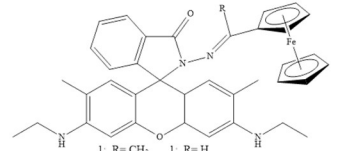| No.	Molecular Structure	Target	Sensing Mechanism	Sensor Type	Detection Limit(M)	Bonding Ratio *	Solution Systems	Application	Ref.
1		Hg^{2+}	/	Colorimetric and fluorescent probe	7.48×10^{-9}	1:2	100% H_2O	Test strip	[33]
2		Hg^{2+}	/	Colorimetric sensor	/	1:1	CH_3CN/H_2O (1/99, *v/v*) HEPES buffer (pH = 7.05)	Actual water samples, living cells	[34]
3		Hg^{2+}	/	Fluorescent and colorimetric sensor	8.73×10^{-7}	/	DMF	Living cells	[35]
4		Hg^{2+}	/	Fluorescent and colorimetric sensor	1.36×10^{-7}	1:1	CH_3CN/H_2O (3/7, *v/v*)	Actual water samples and test paper	[36]

Table 1. *Cont.*

No.	Molecular Structure	Target	Sensing Mechanism	Sensor Type	Detection Limit(M)	Bonding Ratio *	Solution Systems	Application	Ref.
5		Hg^{2+}	/	Fluorescent and colorimetric sensor	0.11×10^{-9}	1:1	EtOH/H_2O (2/1, *v/v*)	Actual water samples, MCF-7 cells, zebrafish and soybean rhizome tissues	[37]
6		Hg^{2+}	/	Fluorescent sensor	/	1:1	/	Living cells	[38]
7		Hg^{2+}	/	Fluorescent and colorimetric sensor	1.8×10^{-8} 1.6×10^{-8} 5.6×10^{-8}	1:1	Tris-HCl/C_2H_5OH (3/7, *v/v*, pH = 7.2)	Living cells	[39]
8		Hg^{2+}	/	Fluorescent sensor	/	1:1	C_2H_5OH/PBS buffer (2/8, *v/v*, pH = 7.4)	Living cells	[40]

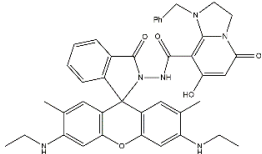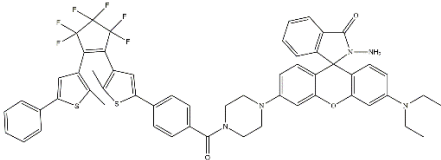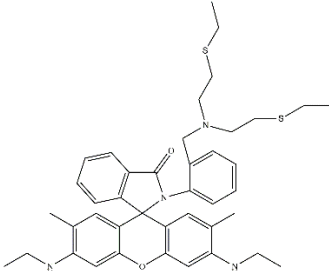<div style="text-align: center">**Table 1.** *Cont.*</div>

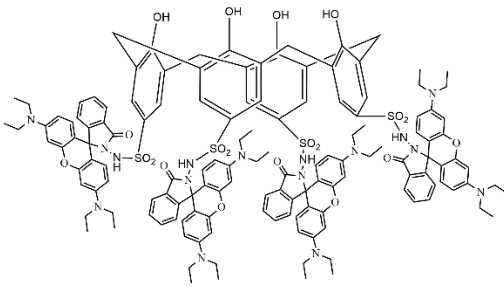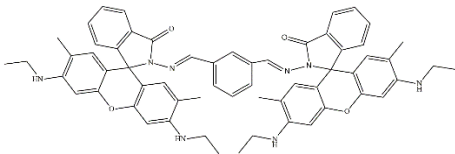| No.	Molecular Structure	Target	Sensing Mechanism	Sensor Type	Detection Limit(M)	Bonding Ratio *	Solution Systems	Application	Ref.
9		Hg^{2+}	/	Fluoric-metric sensor	2.57×10^{-6}	1:1	EtOH/HEPES buffer (1:1, *v/v*)	Test paler and living cells	[41]
10		Hg^{2+}	FRET	Fluorescent and colorimetric sensor	2.46×10^{-7}	1:1	/	Water sample	[42]
11		Hg^{2+}	/	Fluorescent sensor	0.27 µg/L	1:1	/	Water sample	[43]
12		Hg^{2+}	/	Fluorescent and colorimetric sensor	3.4×10^{-9}	1:1	HEPES/DMF (1/1, *v/v*)	Living cells	[44]

Table 1. *Cont.*

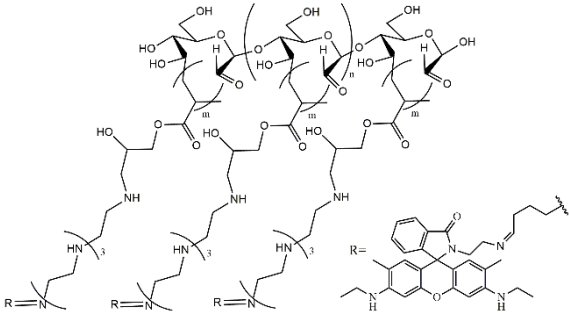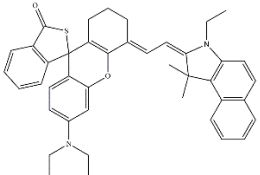| No.	Molecular Structure	Target	Sensing Mechanism	Sensor Type	Detection Limit(M)	Bonding Ratio *	Solution Systems	Application	Ref.
13		Hg^{2+}	/	Fluorescent and colorimetric sensor	1.2×10^{-8}	1:1	CH_3CN/H_2O (9:1*v/v*)	Test strip	[45]
14		Hg^{2+}	/	Fluorescent and colorimetric sensor	9.18×10^{-7}	1:1	/	Tap water, colorimetric card	[46]
15		Hg^{2+}	/	Fluorescent sensor	/	2:1	H_2O/EtOH (3/2, *v/v*, pH = 7.3);	Living cells	[47]

Table 1. *Cont.*

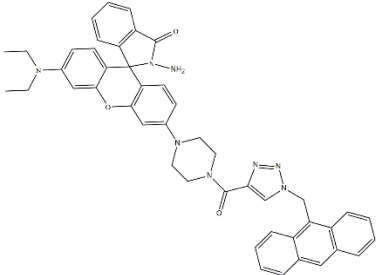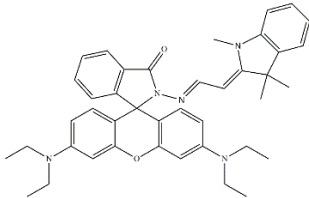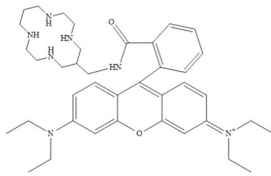| No.	Molecular Structure	Target	Sensing Mechanism	Sensor Type	Detection Limit(M)	Bonding Ratio *	Solution Systems	Application	Ref.
16		Hg^{2+}	FRET	Colorimetric and ratiometric fluorescent sensor	0.81×10^{-6}	1:1	CH_3CN/H_2O (1/1, *v/v*)	Living cells	[48]
17		Cu^{2+}	FRET	Colorimetric and ratiometric probe	1.168×10^{-8}	1:1	CH3CN/HEPES buffer (4/1, *v/v*) (pH = 7.3)	Actual water samples	[24]
18		Cu^{2+}	/	Fluorescent sensor	4.38×10^{-8}	1:1	H_2O	White wine samples	[49]

Table 1. *Cont.*

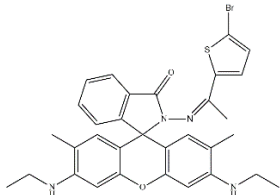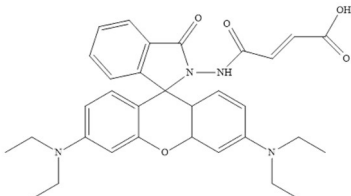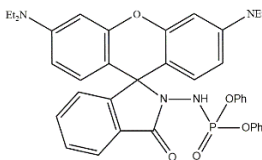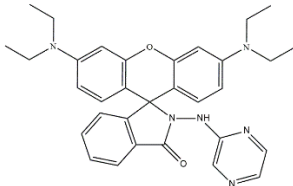| No.	Molecular Structure	Target	Sensing Mechanism	Sensor Type	Detection Limit(M)	Bonding Ratio *	Solution Systems	Application	Ref.
19		Cu^{2+}	PET	Fluorescent and colorimetric sensor	7.4×10^{-8}	1:1	H_2O/DMSO (9/1, *v/v*)	Test paper	[50]
20		Cu^{2+}	/	Fluorescent and colorimetric sensor	0.69×10^{-8}	1:2	Acetone/H_2O (1/2, *v/v*)	Living cells	[51]
21		Cu^{2+}	/	Fluorescent and colorimetric sensor	/	1:1	HEPES /CH_3CN (4/1, *v/v*) (pH = 7.0)	Living cells	[52]
22		Cu^{2+}	/	Fluorescent and colorimetric sensor	8.99×10^{-8}	1:2	CH_3CN/H_2O (1/2, *v/v*) (pH = 7.2, 50 mM tris–HCl)	HepG2 living cells	[53]

Table 1. *Cont.*

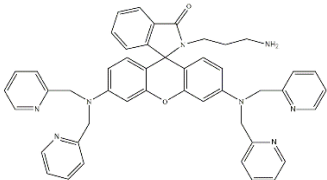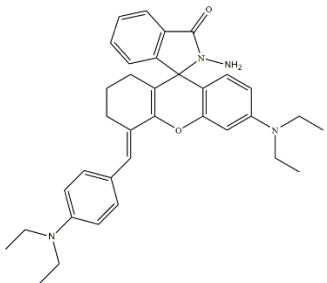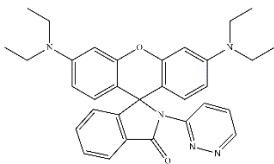| No.	Molecular Structure	Target	Sensing Mechanism	Sensor Type	Detection Limit(M)	Bonding Ratio *	Solution Systems	Application	Ref.
23		Cu^{2+}	/	Fluorescent and colorimetric sensor	3.4×10^{-8}	1:2	CH_3OH/H_2O (4:1, *v/v*)	Gel balls	[54]
24		Cu^{2+}	ICT	Fluorescent sensor	6×10^{-6}	2:1	PBS/EtOH (1/1, *v/v*)	/	[27]
25		Fe^{3+}	/	Colorimetric sensor	2.54×10^{-8}	1:1	EtOH/H_2O (5/5, *v/v*) Tris–HCl (pH = 7.4)	Living cells	[32]
26		Fe^{3+}	/	Fluorescent and colorimetric sensor	3.76×10^{-9}	1:1	MeCN/H_2O (1/1, *v/v*) (pH = 7.2)	Living cells	[55]

Table 1. *Cont.*

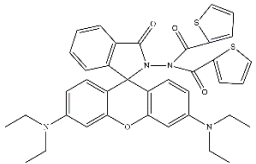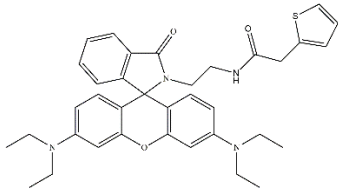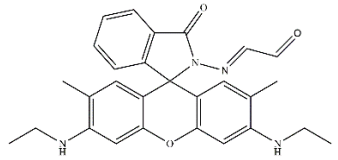| No.	Molecular Structure	Target	Sensing Mechanism	Sensor Type	Detection Limit(M)	Bonding Ratio *	Solution Systems	Application	Ref.
27		Fe^{3+}	/	Fluorescent and colorimetric sensor	2.7×10^{-7}	2:1	EtOH/H_2O (2/3, *v/v*) (pH = 7.2)	Living cells	[56]
28		Fe^{3+}	/	Fluorescent and colorimetric sensor	7.4×10^{-6}	2:1	CH_3CN/ Tris–HCl buffer (9/1, *v/v*; pH = 7.00)	Actual water samples	[57]
29		Fe^{3+}	/	Fluorescent sensor	5.2×10^{-6}	1:1	Acetonitrile/ Tris-HCl buffer (3/7, *v/v*; pH = 7.4)	Living cells	[58]
30		Fe^{3+}	/	Fluorescent sensor	1.64×10^{-6}	1:1	Pure water	Water	[59]

Table 1. *Cont.*

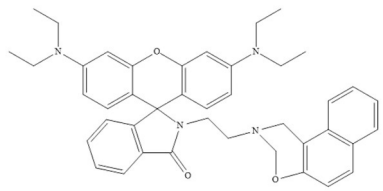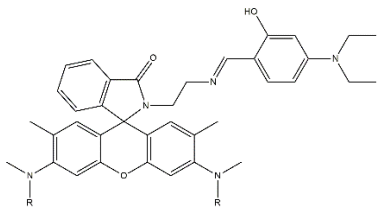| No.	Molecular Structure	Target	Sensing Mechanism	Sensor Type	Detection Limit(M)	Bonding Ratio *	Solution Systems	Application	Ref.
31		Fe^{3+}	/	Colorimetric sensor	0.88×10^{-7}	/	Polyacrylamide	Water	[60]
32		Fe^{3+}	/	Fluorescent and colorimetric sensor	/	1:1	/	/	[61]
33		Fe^{3+}	/	Fluorescent sensor	3.47×10^{-9}	/	HEPES/ CH$_3$CN (2:3, *v/v*) (10 mM, pH = 7.4)	Caenorhabditis elegans, adult mice, plant tissue	[62]
34		Fe^{3+}	/	Fluorescent and colorimetric sensor	0.19×10^{-9}	/	Rhodamine-grafted paper	Environmental water	[63]

Table 1. *Cont.*

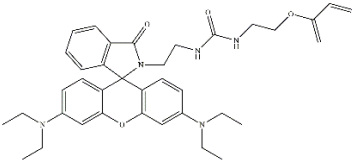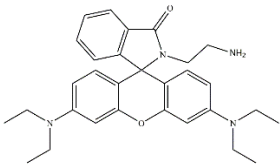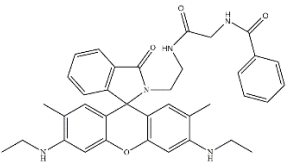| No.	Molecular Structure	Target	Sensing Mechanism	Sensor Type	Detection Limit(M)	Bonding Ratio *	Solution Systems	Application	Ref.
35		Fe^{3+}	FRET	Fluorescent sensor	3.90×10^{-8}	/	Dioxane/H_2O (4:6, *v/v*)	Paper test strips, water samples	[29]

Table 1. *Cont.*

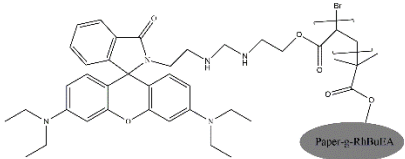| No.	Molecular Structure	Target	Sensing Mechanism	Sensor Type	Detection Limit(M)	Bonding Ratio *	Solution Systems	Application	Ref.
36		Fe^{3+}	ICT	Fluorescent and colorimetric sensor	3.16×10^{-6}	1:2	H_2O (pH = 6.5)	Living cells, fetal bovine serum samples	[28]
37		Pb^{2+}	PET	Colorimetric sensor	4.2×10^{-9}	1:1	EtOH/H_2O (3/2, *v/v*) HEPES Buffer (pH = 7.4)	Living cells, test paper	[25]
38		Pb^{2+}	PET	Fluorescent and colorimetric sensor	0.17×10^{-9}	1:1	CH_3OH/PBS buffer (1/1, *v/v* pH = 7.40)	Living cells	[26]
39		Pb^{2+}	/	Fluorescent and colorimetric sensor	2.5×10^{-6}	1:1	/	Tap water, soil, fish, shrimp	[64]

Table 1. *Cont.*
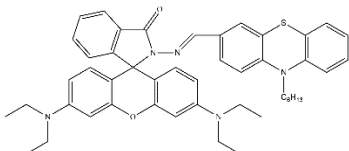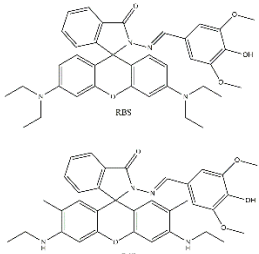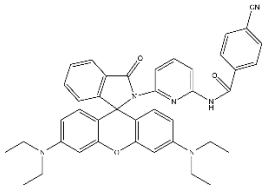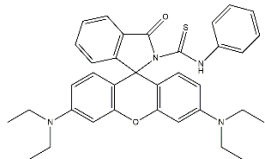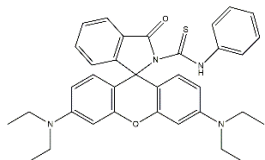
No.	Molecular Structure	Target	Sensing Mechanism	Sensor Type	Detection Limit(M)	Bonding Ratio *	Solution Systems	Application	Ref.
40		Zn^{2+}	FRET	Fluorescent sensor	2.89×10^{-8}	1:1	H_2O /Acetonitrile (8/2, v/v)	Living cells	[65]
41		Zn^{2+}	ICT	Fluorescent sensor	$1.8–1.9 \times 10^{-9}$	/	50 mM, HEPES buffer, pH = 7.54	Living cells, mitochondria	[66]
42		As^{3+}	/	Fluorescent and colorimetric sensor	0.164 µg/L	/	Acetonitrile/ HEPES buffer (4/1, *v/v*, pH = 7.4)	Living cells	[67]

Table 1. *Cont.*

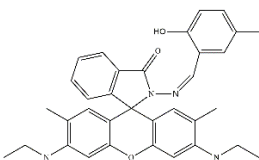| No.	Molecular Structure	Target	Sensing Mechanism	Sensor Type	Detection Limit(M)	Bonding Ratio *	Solution Systems	Application	Ref.
43		Al^{3+}	/	Fluorescent sensor	0.146×10^{-6}	1:1	/	Living cells, plant cells and living bodies	[68]
44		Cr^{3+}	/	Fluorescent sensor	/	1:1	/	Living cells	[69]
45		Sn^{2+}	ICT	Fluorescent and colorimetric sensor	1.62×10^{-7}	1:1	EtOH/H$_2$O (8/2, *v/v*)	Living cells	[70]

*: The bonding ratio is between probe and target.

2.1. Rhodamine-Based Sensors for Hg^{2+}

A rhodamine-fluorene-based dual channel sensor was synthesized for selective detection of Hg^{2+} via both colorimetry and fluorometry (Table 1, No. 1), and the sensor's solubility was greatly improved by the alkyl chain in the fluorene moiety, enabling its utility in 100% H$_2$O [33]. The prepared sensor selectively detected Hg^{2+} in 100% water using a strip with a good response and was then used as a digital printing material.

Hong M., et al. synthesized a spectral sensor through a one-step reaction between rhodamine B and thiobisethylamine, named 2-(2-((2-aminoethyl)thio)ethyl)-3′,6′-bis(diethylamino)spiro [isoindoline-1,9′-xanthen]-3-one (RMTE) (as shown in Table 1, No. 2) [34]. RMTE emitted a new fluorescence peak at 578 nm in the presence of Hg^{2+} with a remarkable visual change in fluorescence color (Figure 2).
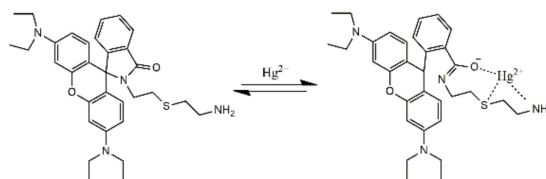

Figure 2. The proposed sensing mechanism of RMTE (Table 1, No. 2) for Hg^{2+} [34].

Cicekbilek, F. et al., reported a Hg^{2+} sensor synthesized a facile Schiff base-type reaction between 9-anthraldehyde and aminated rhodamine [35] and used to detect Hg^{2+} with observable sensitivity and selectivity via colorimetric and fluorescence methods (Table 1, No. 3). The detection limit of the proposed sensor was 0.87 μM. The sensing mechanism of the as-prepared sensor to Hg^{2+} was based on a spirolactam ring-opening reaction, verified through UV-Vis, FTIR, and NMR titration analyses.

A promising colorimetric and fluorometric chemosensor named RDV was designed by Patil S. K., et al. for specific detection of Hg^{2+} (Table 1, No. 4) [36]. The color of the "turn-on" fluorescence sensor changed from colorless to pink before and after the addition of Hg^{2+} in an aqueous acetonitrile medium (Figure 3). The sensing limit of RDV for Hg^{2+} was 136 nM, revealing a high sensitivity of the sensor.
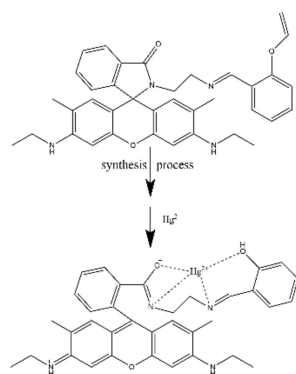
Figure 3. The possible mechanism of RDV (Table 1, No. 4) to Hg^{2+} [36].

Kan, C. et al. constructed a novel reversible fluorescent probe named RBST (Table 1, No. 5), by the reaction of 2-thiopheneacetyl chloride and rhodamine B, [37]. RBST showed a sensitive and selective response to Hg^{2+} in EtOH/H$_2$O (2,1, *v/v*) with the detection limit of 0.11 μM (Figure 4). The reversibility of RSBT was attributed to the strong affinity of S^{2-} and Hg^{2+}. Besides, the RSBT was used to detect Hg^{2+} in real water samples, suggesting its promising practicality.

Figure 4. The proposed sensing mechanism of RBST (Table 1, No. 5) to Hg^{2+} [37].

Dewangan S., et al. synthesized a significant molecule through the functioning of the cymantrenyl hydrazone system by fluorescent tagging of rhodamine (Table 1, No. 6) [38]. The synthesized molecule displayed high selectivity and responsiveness to Hg^{2+} (Figure 5). The prepared sensor was applied to recognize Hg^{2+} in bacterial strains and THP-1 cancer cells, indicating its potential in bioimaging applications.

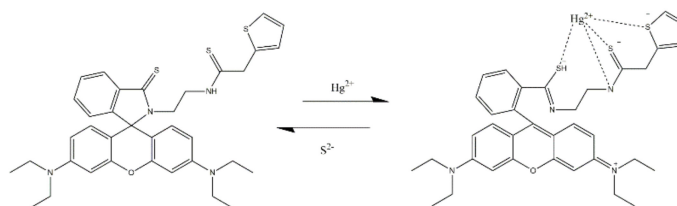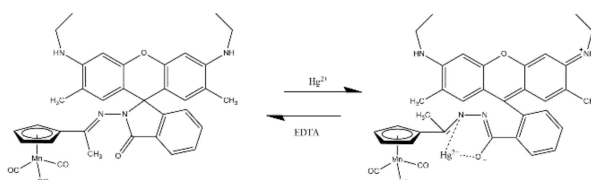**Figure 5.** The possible sensing mechanism of the prepared sensor (Table 1, No. 6) to Hg^{2+} [38].

Wang Q., et al. synthesized three rhodamine based probes 1, 2, and 3 (Table 1, No. 7) and applied them for Hg^{2+} detection in Tris-HCl/C_2H_5OH (v:v = 3:7, 10 mM, pH = 7.2). All three probes were colorless at first but turned to visible pink after the addition of Hg^{2+} with the fluorescence increment. The detection limits of probes 1, 2, 3 to Hg^{2+} were 18 nM, 16 nM, 56 nM, respectively. These probes were successfully applied to both environmental samples and bioimaging applications, as shown in Figure 6.
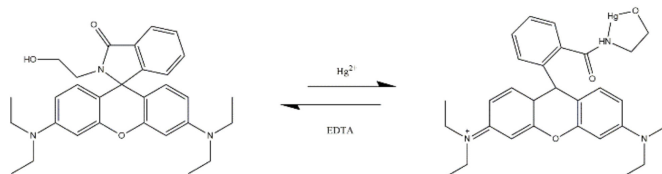
Figure 6. The possible mechanism of Probe 2 (Table 1, No. 7) to Hg^{2+} [39].

A ferrocene-based rhodamine-hydrazone molecular probe (Table 1, No. 2) was synthesized using the solid-state synthetic method by Dewangan S., et al. [40]. The probe showed selective recognition of Hg^{2+}. It was therefore applied to intracellular metal detection and bioaccumulation analysis, showing its promising application prospects. The proposed sensing mechanism of the prepared probe to Hg^{2+} was shown in Figure 7.
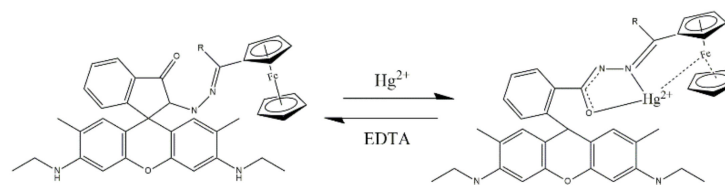
Figure 7. The proposed sensing mechanism of the prepared probe (Table 1, No. 8) to Hg^{2+} [40].

Gauthama B. U., et al. designed a rhodamine-based sensor named RhB, with a selective and sensitive response for Hg^{2+} (Table 1, No. 9) [41]. The UV-Vis and fluorescence spectral profiles changed in the presence of Hg^{2+} due to the formation of the coordinate bond between RhB and Hg^{2+} (Figure 8). The detection limit was around 2.57×10^{-6} M and the prepared sensor detected Hg^{2+} in 100% aqueous solution by the naked eye.

Figure 8. The possible sensing mechanism of RhB (Table 1, No. 9) to Hg^{2+} [41].

Li, X., et al. synthesized a fluorometric and colorimetric chemosensor, named 1O and studied its responses for Hg^{2+} (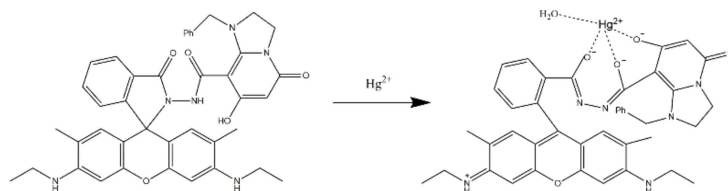Table 1, No. 10). The results suggested that Hg^{2+} induced remarkable colorimetric and fluorescent changes, due to the reaction between 1O and Hg^{2+} (Figure 9). Singh S., et al. described a rhodamine-based fluorescence sensor for Hg^{2+} detection in water samples (Table 1, No. 11) [43]. The influences of different analytical parameters on the analytical performance of the sensors were discussed. Results showed that replacing the fluorophore of rhodamine B with rhodamine 6G on the prepared sensor improved the limit of detection. In addition, the buffer optimization improved detection limits and selectivity. The prepared sensor was successfully applied for Hg^{2+} detection in tap and river samples.
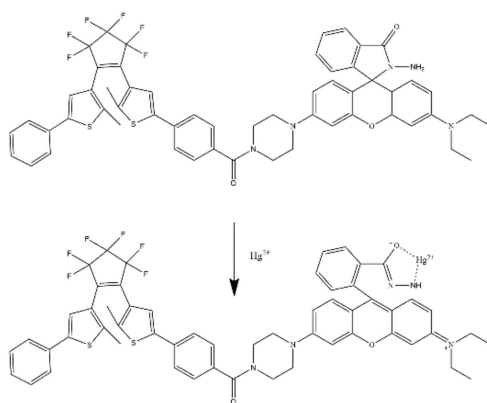
Figure 9. The proposed reaction mechanism between 1O (Table 1, No. 10) and Hg^{2+} [42].

Yilmaz, B., et al. [44] reported a novel rhodamine-based sensor, using the calixarene as the skeleton and appended with four rhodamine units at the upper rim (Table 1, No. 12). The prepared sensor showed high selective and sensitive response to Hg^{2+} with immediately turning on fluorescence output. Through in vitro and bio-imaging studies, the prepared sensor was cell permeable and suitable for real-time imaging of Hg^{2+} in living cells. Aduroja O., et al. synthesized a rhodamine-based sensor, RD6 (Table 1, No. 13) [45], with excellent selectivity sensitivity to Hg^{2+} in an aqueous buffer solution by colorimetric and fluorescent methods. The detection limit of RD6 for Hg^{2+} was 1.2×10^{-8} M. With the CN^- assistance, the prepared sensor realized reversibility due to the strong stability of $Hg(CN)_2$ (Figure 10).
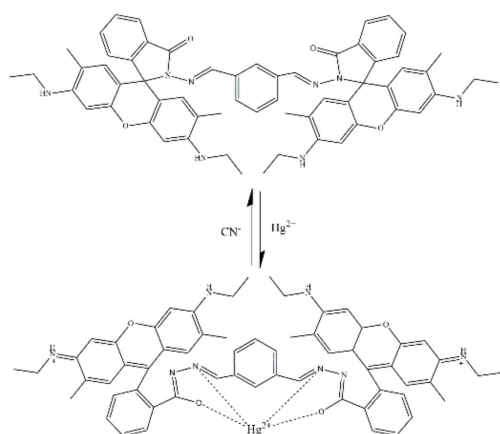
Figure 10. The proposed sensing mechanism of RD6 (Table 1, No.13) to Hg^{2+} [45].

Li M., et al. constructed a novel rhodamine-based material, FFC, for the detection and adsorption of Hg^{2+} (Table 1, No. 14) [46]. The cellulose was chosen as the skeleton and the rhodamine moiety was conjugated with cellulose as the recognition group, enabling excellent optical signals in the presence of Hg^{2+}. After adding Hg^{2+}, the intensity of fluorescence enhancement of FFC showed a 7-fold enhancement by triggering the spirolactam ring-opening reaction. The adsorption process of FFC to Hg^{2+} was fitted with the Langmuir adsorption model and pseudo-second-order kinetics. The prepared FFC was successfully applied for the detection and adsorption of Hg^{2+} in tap water. Liang F. et al. introduced an anthocyanin functional group in the rhodamine spiro ring and constructed a sensitive and selective near-infrared (NIR) fluorescent sensor, CCS-Hg for Hg^{2+} (Table 1, No. 15) [47]. The prepared CCS-Hg was applied to determine Hg^{2+} distribution in living cells. The sensing mechanism was verified through theoretical calculations (Figure 11).
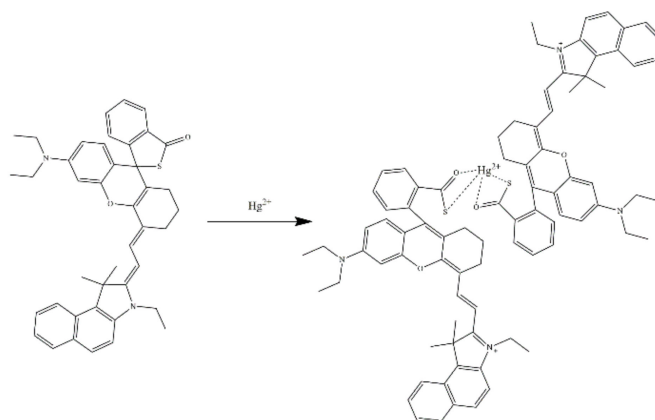
Figure 11. The proposed sensing mechanism of CCS-Hg (Table 1, No. 15) [47].

Zhang Q., et al. designed a rhodamine-based sensor for selective detection of Hg^{2+} via the FRET mechanism (Table 1, No. 16) [48]. The synthesized material possessed great pseudo-Stokes (174 nm) in the presence of Hg^{2+} and showed fluorescent and ratiometric response with a fast reaction time (less than 30 s) (Figure 12). The limit of detection for Hg^{2+} was found to be 0.38 $\times$ 10^{-6} M.
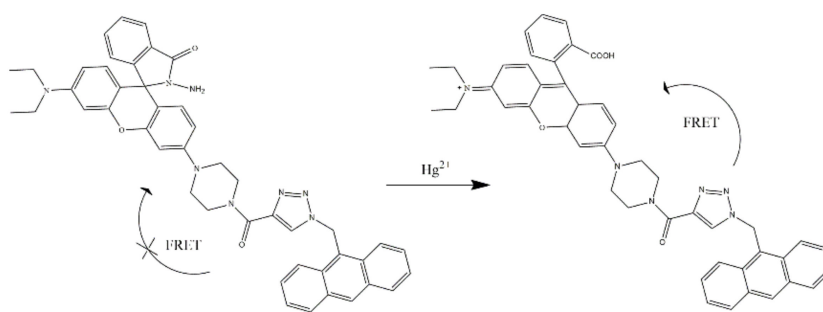
Figure 12. The proposed sensing mechanism of the prepared sensor (Table 1, No. 16) for Hg^{2+} [48].

2.2. Rhodamine-Based Sensors for Cu^{2+}

Zhang J., et al. constructed a FRET-based sensor for the detection of Cu^{2+} (Table 1, No. 17) [24], by conjugating rhodamine with a 2-(1,3,3-trimethylindolin-2-ylidene) acetaldehyde moiety. The designed sensor demonstrated colorimetric and ratiometric responses to Cu^{2+} with a detection limit of 1.168×10^{-8} M (Figure 13). The prepared sensor was successfully applied to detect Cu^{2+} by test paper strips and in real water samples.
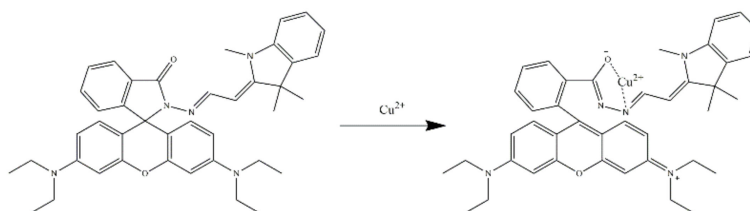
Figure 13. The proposed sensing mechanism of the prepared sensor (Table 1, No. 17) [24].

During grape wine production, copper could disorientate volatile sulfur compounds and cause turbidity formation, thus lowering the wine quality [71]. By decorating rhodamine B with a tetra azamacrocyclic ring, a probe was created to monitor the Cu^{2+} in wine with a detection limit of 4.38×10^{-8} M (Table 1, No.18) (Figure 14) [49]. The prepared sensor responded to Cu^{2+} only in acidic conditions (< pH 5.5).
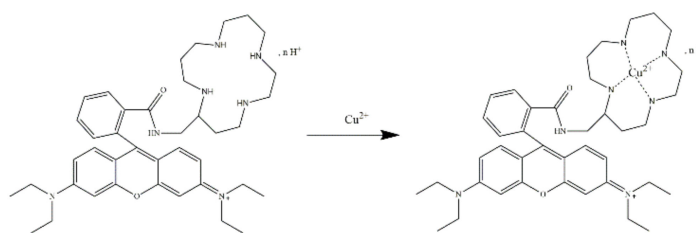
Figure 14. The proposed reaction mechanism of the prepared sensor (Table 1, No.18) [49].

Deepa A., et al. synthesized a fluorescent and colorimetric sensor, named 6GS2, exhibiting a specific response after binding with Cu^{2+} (Table 1, No.19) [50]. The spirocyclic structure of 6GS2 transformed into a non-cyclic form in the presence of Cu^{2+} and the fluorescent peak intensity increased in the H$_2$O/DMSO (9/1, *v/v*) medium. The fluorescence intensity increments of 6GS2 induced by Cu^{2+} is attributed to the PET mechanism (Figure 15).
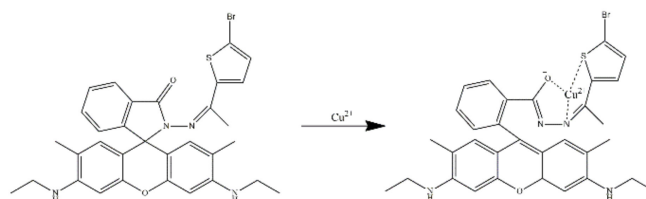
Figure 15. The proposed mechanism of 6GS2 (Table 1, No. 19) for sensing Cu^{2+} [50].

Hosseinjani-Pirdehi H., et al., prepared a biocompatible fluorogenic chemosensor named RHA (Table 1, No. 20) [51]. Furan-2,5-dione and rhodamine combined with an iminohydrazine crosslinker were the receptor and fluorophore of RHA, respectively. The RHA served as a pH indicator in acidic media and a sensitive sensor with high selectivity to Cu^{2+} RHA was used for bio-imaging applications in acidic and neutral pH. A novel sensor, named RhP, was synthesized by integrating the rhodamine phosphonate group (Table 1, No. 21) [52]. RhP demonstrated highly sensitive and selective recognition for Cu^{2+} and the detection limit of RhP was 15×10^{-6} M. The sensing of Cu^{2+} by RhP was achieved in less than 15 s (Figure 16).
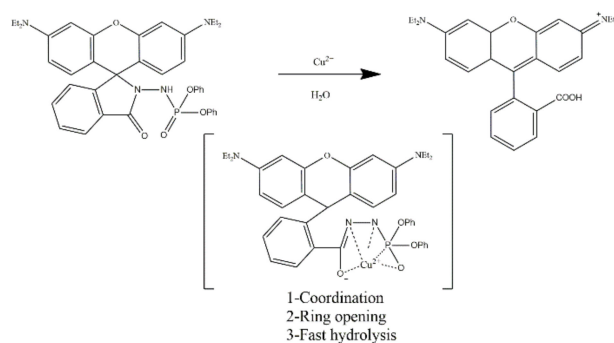

Figure 16. The proposed detecting mechanism of RhP (Table 1, No. 21) [52].

Wang Y., et al. synthesized a naked-eye and fluorescent chemosensor, by introducing pyrazinyl hydrazine in rhodamine B, for Cu^{2+} detection (Table 1, No. 22) [53]. The sensor color changed from colorless to amaranth after Cu^{2+} addition. The proposed response mechanism of the prepared sensor (Figure 17) was extrapolated through the results of mass spectra, fluorescence spectra, and theoretical calculations.
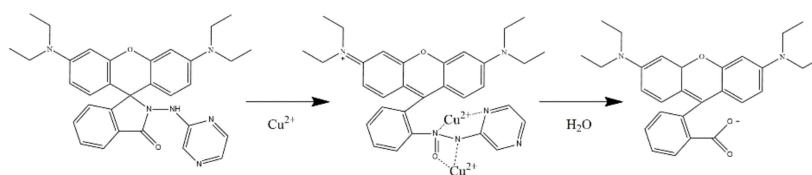
Figure 17. The proposed response mechanism of the prepared sensor (Table 1, No. 22) for Cu^{2+} [53].

Yang L., et al. reported a novel rhodamine-based sensor, poly-NRG, modified by picolyl groups serving as the recognizing ligand for Cu^{2+} (Table 1, No. 23) [54]. The prepared poly-NRG was further modified into gel balls for the Cu^{2+} adsorption which showed a specific reaction in the presence of Cu^{2+} with obvious color changes and achieved recycling after treatment with EDTA solution (Figure 18). Hu L., et al. reported a NIR fluorescent sensor EtRh-N-NH$_2$ employing rhodamine as a fluorescent core and a hydrazine group as a responsive site for Cu^{2+} (Table 1, No. 24) [27]. The sensitivity and selectivity of the prepared sensor turned out to be satisfactory with the low detection limit (6×10^{-6} M). The proposed sensing mechanism was shown in Figure 19. Furthermore, EtRh-N-NH$_2$ was used in the bio-imaging of Cu^{2+} in living cells.

Figure 18. The proposed sensing process of NRG (Table 1, No. 23) [54].

Figure 19. The proposed sensing mechanism of EtRh-N-NH$_2$ (Table 1, No. 24) [27].

2.3. Rhodamine-Based Sensors for Fe^{3+}

Cheng Z., et al. synthesized a rhodamine-based sensor, named J1, for Fe^{3+} detection (Table 1, No. 25) [32]. The colorless sensor solution visibly turned pink in the presence of Fe^{3+}, realizing the detection of Fe^{3+} in an aqueous environment. The prepared sensor was successfully used in the bio-imaging of Fe^{3+} in living cells, indicating its promising application prospects. Liu Y., et al. synthesized an N, N-dithenoyl-rhodamine-based sensor for fluorescent and colorimetric Fe^{3+} detection (Table 1, No. 26) [55]. The excellent selectivity of the prepared sensor was attributed to the coordinating functional recognition group of two thiophene carbonyl groups and the detection limit was around 3.76×10^{-9} M (Figure 20). The reported sensor also exhibited satisfactory membrane permeability and was also used for bio-imaging in living cells.
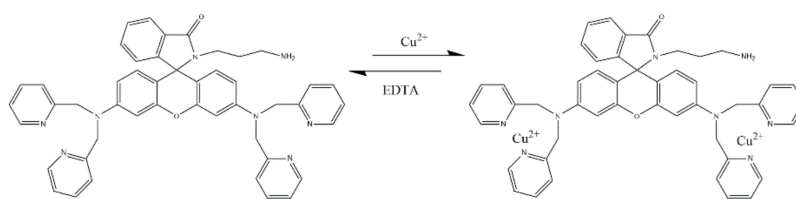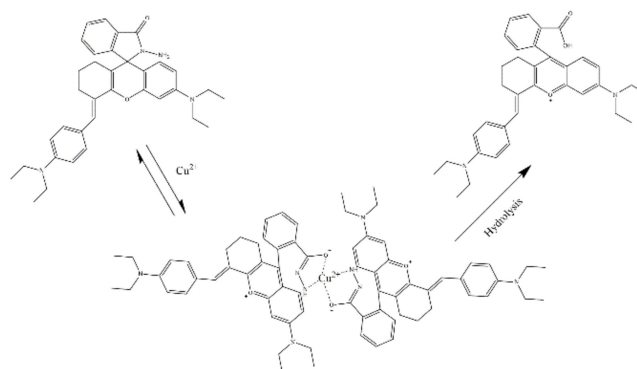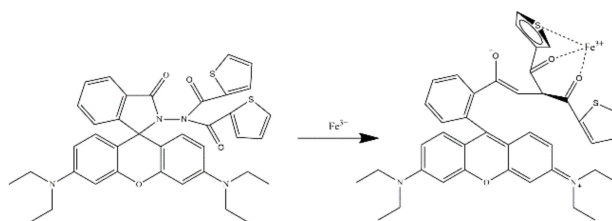

Figure 20. The proposed sensing mechanism of the prepared sensor (Table 1, No. 26) to Fe^{3+} [55].

Wang K. P., et al. (Table 1, No. 27) reported a Fe^{3+}-detecting fluorescence sensor, BYY, synthesized by the reaction of 2-thiopheneacetic acid and N-(rhodamine-B)lactam-ethylenediamine [56]. The BYY sensor exhibited high sensitivity toward Fe^{3+} in EtOH/H$_2$O (2/3, *v/v*, pH = 7.2) with a fast response rate. Owing to a strong affinity between Na$_4$P$_2$O$_7$ and Fe^{3+}, BYY realized the reversible binding of Fe^{3+} (Figure 21). BYY was successfully applied for the bio-imaging of Fe^{3+} in living cells.

Figure 21. The proposed sensing mechanism of BYY (Table 1, No. 27) for Fe^{3+} [56].

Wang, Y., et al. designed a simple rhodamine-based fluorescent and colorimetric sensor, L1, exhibiting a good selectivity and sensitivity to Fe^{3+} (Table 1., No. 28) [57]. The detection limit of the L1 sensor was 0.29×10^{-6} M. The sensing process, which was shown in Figure 22, was chemically reversible at least three times on the alternate addition of AcO^- and Fe^{3+}.
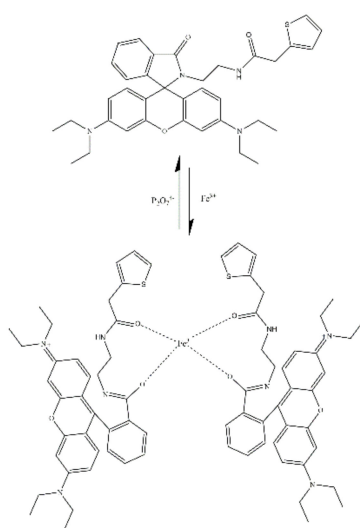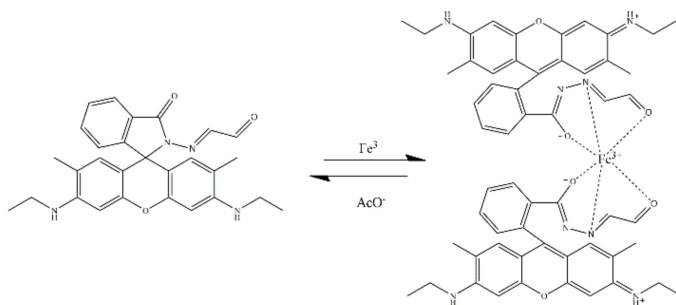

Figure 22. The proposed sensing mechanism of the prepared sensor L1 (Table 1, No. 28) to Fe^{3+} [57].

Zhang M., et al. synthesized four rhodamine-based sensors through simple, high yield, and one-step Mannich reactions, and the acquired product M3 (Table 1, No. 29) exhibited a specific and sensitive response to Fe^{3+} in acetonitrile/Tris-HCl buffer solution (3:7, *v*/*v*; pH = 7.4) (Figure 23) [58]. The prepared Fe^{3+} sensor was successfully applied in bio-imaging by confocal laser scanning microscopy.
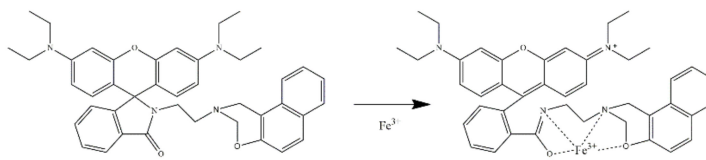
Figure 23. The proposed sensing mechanism of M3 (Table 1, No. 29) to Fe^{3+} [58].

A rhodamine salicylaldehyde sensor, named RS, was constructed to modify a fluorescent PU foam named PU-RS, as a sensitive fluorescence sensor for Fe^{3+} (Table 1, No. 30) [59]. PU-RS showed ring-opened amide form and higher fluorescence intensity, due to the coordination between RS and Fe^{3+} in pure water (Figure 24). Liu X., et al. synthesized a rhodamine-based sensor (RhBUEA) by functionalizing the polyacrylamide hydrogel through free radical polymerization of RhBUEA and then constructed a fast, visual detection device for Fe^{3+} (Table 1, No. 31) [60]. The fabricated hydrogel showed good selectivity

and sensitivity to Fe^{3+} in the pH range of 4.95 to 8.02 with a fast response time (less than 20 min). The prepared device was successfully used for Fe^{3+} detection in real environmental water samples.

Figure 24. The proposed binding mechanism of RS (Table 1, No. 30) to Fe^{3+} [59].

A novel rhodamine-based sensor (RhB-EDA) was constructed by functionalizing rhodamine with the Fe^{3+} recognition group ethylenediamine (EDA) (Table 1, No. 32) [61]. The colorless and non-fluorescent RhB-EDA turned pink and showed high fluorescence in the presence of Fe^{3+} through the coordination-induced lactam ring opening mechanism (Figure 25).
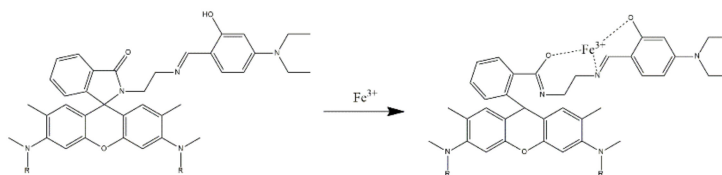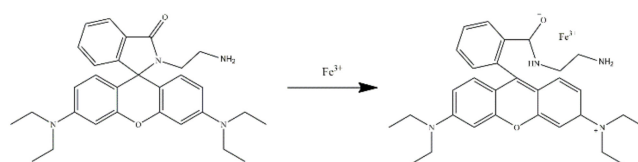

Figure 25. The proposed sensing mechanism of RhB-EDA (Table 1, No. 32) for Fe^{3+} [61].

Zhang J., et al. reported a rhodamine-based sensor named LXY (Table 1, No. 33) for quantitative and qualitative Fe^{3+} detection in HEPES buffer (10 mM, pH = 7.4)/CH_3CN (2:3, v/v) [62]. The detection limit of the LXY sensor for Fe^{3+} was 3.47×10^{-9} M. The prepared sensor achieved a visual detection of Fe^{3+} through the color and fluorescence change before and after the addition of Fe^{3+} (Figure 26) and was successfully used in bio-imaging of Caenorhabditis elegans, adult mice, and plant tissue.
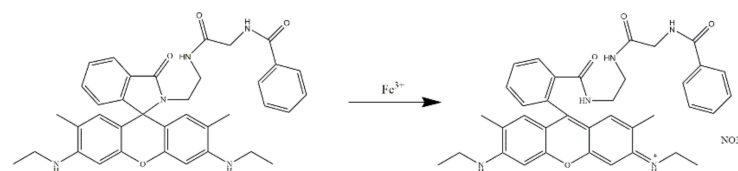
Figure 26. The proposed sensing mechanism of LXY (Table 1, No. 33) to Fe^{3+} [62].

A filter paper grafted with rhodamine B (paper-g-RhBUEA) was reported to detect Fe^{3+} via fluorescent and colorimetric assay by Liu X., et al. (Table 1, No. 34) [63]. The sensor paper-g-RhBUEA realized the on-site detection of Fe^{3+} using a self-developed smartphone mini application named "Colorimetric detector". In addition, the fast visual detecting device paper-g-RhBUEA was successfully applied to the on-site detection of Fe^{3+} in environmental water samples. Cuc T. T. K., et al. designed and synthesized a multi-stimuli responsive rhodamine-based sensor, pseudo [3] rotaxane NI-DBC/RB-DBA (Table 1, No. 35), for the detection of Fe^{3+} [29]. The prepared mono-fluorophoric pseudo [3] rotaxane NI-DBC/RB-DBA transformed into bi-fluorophoric pseudo [3] rotaxane NI-DBC/RB-DBA-Fe^{3+} in the presence of Fe^{3+} by triggering the FRET process (Figure 27). The sensor exhibited high sensitivity to Fe^{3+} with a very low detection limit (3.90×10^{-8} M) and was applied to detect Fe^{3+} in pristine water samples.
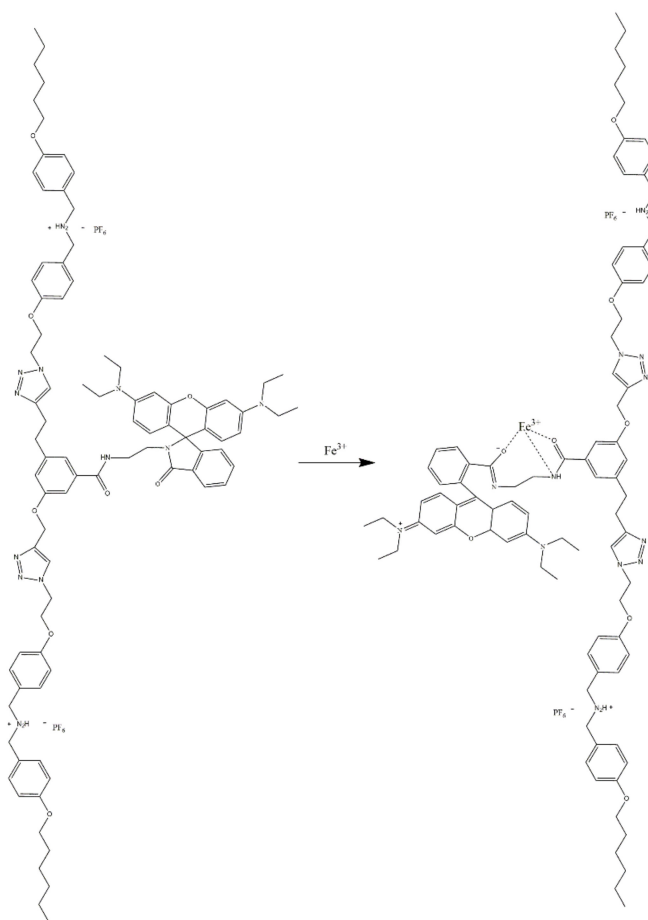
Figure 27. The possible coordination mechanism of pseudo [3]rotaxane NI-DBC/RB-DBA (Table 1, No. 35) with Fe^{3+} [29].

Qiu X., et al. reported a water-soluble rhodamine-poly ethylene glycol (DRF-PEG) conjugated sensor as a dual-responsive sensor for Fe^{3+} detection (Table 1, No. 36) [28]. DRF-PEG was comprised of rhodamine 6G hydrazide and benzaldehyde-functionalized polyethylene glycol and synthesized by Schiff base reaction. The water solubility of this prepared sensor was significantly improved by introducing the PEG segment. The designed sensor was successfully used in ratiometric imaging of Fe^{3+} in living cells and Fe^{3+} detection in fetal bovine serum. The possible sensing mechanism of DRT-PEG is shown in Figure 28.
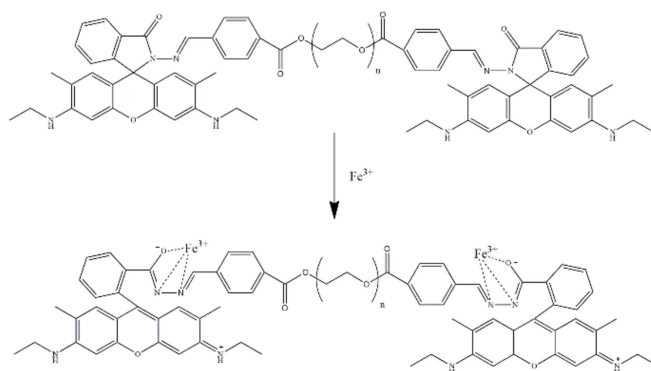
Figure 28. The proposed coordination mechanism of DRF-PEG (Table 1, No. 35) towards Fe^{3+} [28].

2.4. Rhodamine-Based Sensors for Other Metal Ions

A novel rhodamine-based sensor, RBTPA was proposed for the detection of Pb^{2+} by Chen H., et al. (Table 1, No. 37) [25]. This prepared sensor displayed a specific response for Pb^{2+} driven by the PET process and the proposed sensing mechanism is shown in Figure 29. Furthermore, RBPTA was successfully applied to detect Pd^{2+} in actual water samples and living cells. By test paper, RBPTA realizes the on-site and real-time quantitation of Pd^{2+}.
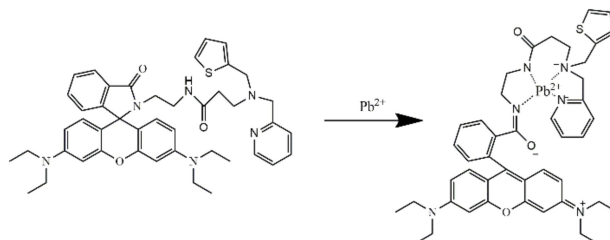
Figure 29. The proposed sensing mechanism of RBTPA (Table 1, No. 37) to Pb^{2+} [25].

Luo M., et al. synthesized a rhodamine-based sensor (R1) by appending indole to rhodamine B (Table 1, No. 38) [26]. The prepared sensor showed a fluorescent and colorimetric response in the addition of Pb^{2+}. The detection limit of R1 for Pb^{2+} was 0.17×10^{-9} M which was suitable for the intra-cellular imaging of Pb^{2+}. Xie X. et al. synthesized a rhodamine 6G hydrazide complex, (R6GH), synthesized for fluorescent and visual detection of Pb^{2+} (Table 1, No. 39) [64] which turned out to be an "off-on" output platform (Figure 30). A paper-based array was also developed by immobilizing R6GH on ordinary filter paper.
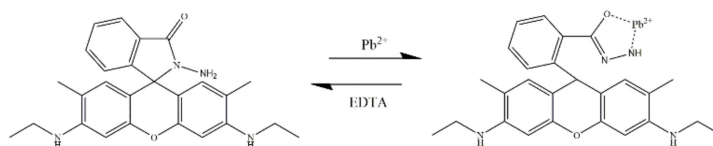
Figure 30. The possible sensing mechanism of R6GH (Table 1, No. 39) to Pb^{2+} [64].

Karmegam M. V., et al. synthesized a phenothiazine–rhodamine (PTRH) sensor for Zn^{2+} sensing in solution and living cells (Table 1, No. 40) [65]. Several factors contributed to the FRET-ON mechanism for Zn^{2+} detection including the spectral overlap of the donor emission band, the phenothiazine groups in PTRH, and the absorption band, the ring-opened of the rhodamine fluorophore group. The possible binding model of PTRH with Zn^{2+} was shown in Figure 31 and the limit of detection of the proposed sensor was 2.89×10^{-8} M.
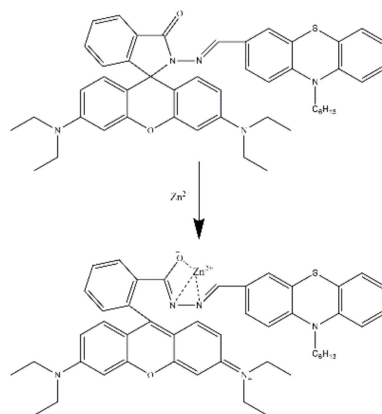
Figure 31. The proposed binding mode of PTRH (Table 1, No. 40) with Zn^{2+} [65].

Zhang X., et al. designed and synthesized both rhodamine-B and rhodamine-based sensors, RBS and R6S (Table 1, No. 41), for Zn^{2+} detection [66] and both sensors showed good selectivity to Zn^{2+}. The pink sensor solution changed to colorless after Zn^{2+} addition with "turn-on" fluorescence enhancement. RBS and R6S were all successfully applied for Zn^{2+} quantification inside mitochondria via fluorescence imaging. Paul S., et al. reported an electronically enriched rhodamine-based sensor, PBCMERI-23, via spirolactam ring opening by As^{3+} (Table 1, No. 42) [67]. The colorless and non-fluorescent PBCMERI-23 turned pink and showed bright yellow fluorescence after the addition of As^{3+} (Figure 32). PBCMERI-23 also exhibited nice cell permeability and was successfully applied to As^{3+} bio-imaging in living cells.
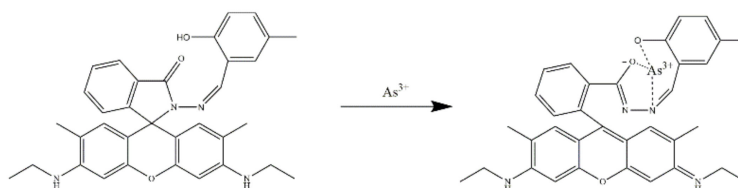

Figure 32. The proposed sensing mechanism of PBCMERI-23 (Table 1, No. 42) to As^{3+} [67].

Kan C., et al. reported a supramolecular fluorescent sensor (RBGP) for Al^{3+} detection (Table 1, No. 43) [68]. The prepared sensor showed a fast and stable response to Al^{3+}. Additionally, the response of RBGP was reversed by the addition of F^- (Figure 33). The prepared sensor was used in Al^{3+} bio-imaging in living cells, plant cells, and animal bodies.
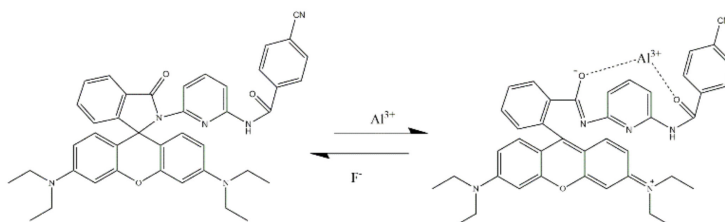
Figure 33. The proposed sensing mechanism of RBGP (Table 1, No. 43) to As^{3+} [68].

RB-CR (Table 1, No. 44), conjugation between rhodamine B and phenylthiourea, was reported by Jiang T. et al. [69]. Spirolactam ring of RB-CR would open when triggered by Cr^{3+} (Figure 34). The UV-Vis absorption and fluorescence signal of RB-CR displayed pronounced enhancement.
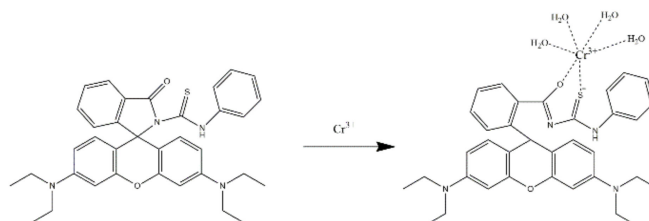
Figure 34. The possible binding mechanism of RB-CR (Table 1, No. 44) to Cr^{3+} [69].

A rhodamine-based sensor (Rh-Hyd) was reported by Rathinam B., et al. (Table 1, No. 45) [70]. The carbonyl and terminal amino groups of Rh-Hyd showed high affinity to Sn^{2+}. The presence of Sn^{2+} induced spirolactam ring-opening reaction of Rh-Hyd and then changed the color and fluorescence of the prepared sensor. The proposed sensing mechanism of Rh-Hyd to Sn^{2+} was shown in Figure 35.
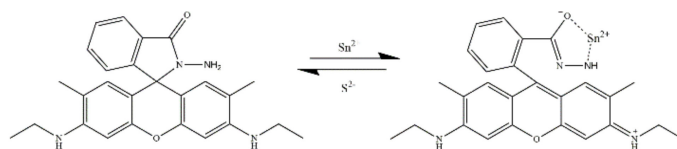
Figure 35. The possible sensing mechanism of Rh-Hyd (Table 1, No. 45) to Sn^{2+} [70].

3. Rhodamine-Based Sensors for H$^+$

It is significant to investigate dynamic pH in living cells since pH is an indicator of the body's health and also plays a critical role in cellular processes, such as cell adhesion, cell growth, and ion transport [72–74]. The design inspiration for the H$^+$ sensor, named Lyso-NIR-pH, was drawn from the certain correlation between heat stroke and lysosome acidity (Table 2, No. 1) [75]. Thus, the probe structured with an openable deoxylactam served as a response group to pH and the morpholine moiety acted as a recognizing unit for lysosome (Figure 36). This sensor acquired photo-bleaching and auto-fluorescence in vivo, revealed by previous similar sensors as a result of the fluorophore, Si-rhodamine with excellent photostable and NIR fluorescence.
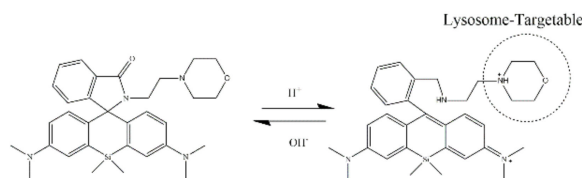

Figure 36. The response mechanism of Lyso-NIR-pH (Table 2, No. 1) to pH in lysosome [75].

Sensor No. 2 (Table 2) was developed for pH changes in lysosomes during induced abnormal cells, thus promoting cellular signaling responses [76]. This pH sensor exhibited excellent selectivity, sensitivity, and water solubility with a pKa value of 4.10. Remarkably, it was reused for five cycles, demonstrating strong and reproducible performances. pH probes with pKa around six were appropriate for monitoring intracellular pH changes and studying cell processes [77].

The NIR fluorescence sensor of pH, based on hydroxymethyl germanium-rhodamine, showed an optimal pKa for the successful visualization of tumors in a mouse model. The proposed sensor was ranked at the top list among similar probes (Table 2, No.3) [78]. In comparison, the three pH-triggered NIR fluorescent probes (Table 2, No.4) with different pKa values (4.4 for Probe No. 4.1, 4.6 for Probe No. 4.2, and 4.8 for Probe No. 4.3) were synthesized with rhodamine dyes and tetraphenylethene used as FRET or through-bond energy transfer (TBET) donors [79]. The ratiometric sensors caused the aggregation-quenching effect, inducing 98.9% energy transfer from TPE to rhodamine and consequently showing excellent photostability and good selectivity for pH.

Yan Y., et al. reported a BODIPY-rhodamine-based sensor, BDP-RhB to measure the variation in pH of lysosomes in macrophages during inflammation (Table 2, No. 5) [80]. Based on FRET, BDP-RhB responded to the pH range of 8.0 to 4.0 (Figure 37). Importantly, the prepared sensor exhibited good lysosome targeting ability and demonstrated a decrease in pH value during inflammation in macrophages.
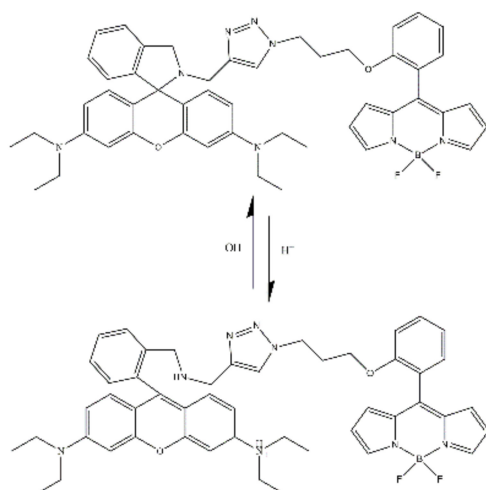
Figure 37. The response mechanism of BDP-RhB (Table 2, No. 5) to pH [80].

A novel aggregation-induced emission target molecule was proposed by Liu Z., et al. (Table 2, No. 6) [81], acquired from rhodamine 6G hydrazine and tetrastyrene carbaldehyde through a high boiling solvent (DMF/H$_2$O) volatilization method. The change in pH induced spiro ring opening structure and the color change (colorless to pink) of the prepared sensor (Figure 38).
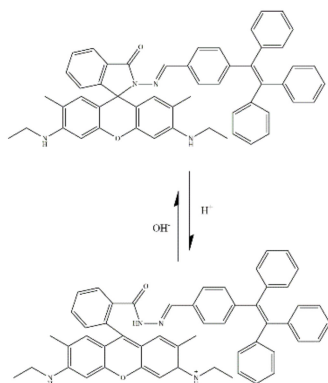
Figure 38. The concluded sensing mechanism of this prepared sensor (Table 2, No. 6) for pH [81].

Table 2. Rhodamine-based sensors for H$^+$.
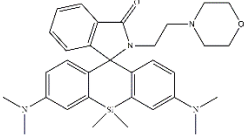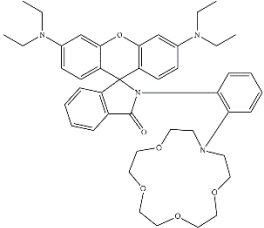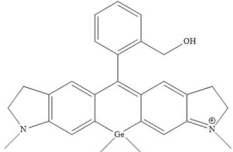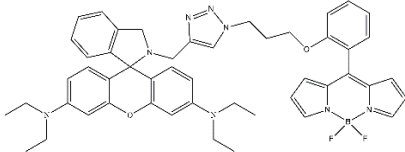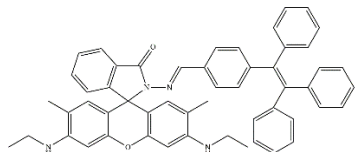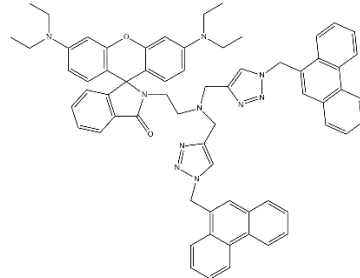
No.	Molecular Structure	Target	Sensing Mechanism	Sensor Type	Sensitive pH Range	pKa	Solution Systems	Application	Ref.
1		H$^+$	/	Fluorescent sensor	/	4.63	/	Living cells	[75]
2		H$^+$	/	Fluorescent sensor	pH = 4.0–7.0	4.10	/	Living cells	[76]
3		H$^+$	/	Fluorescent sensor	/	6.24	NaPi buffer	Living cells	[78]
4		H$^+$	TBET and FRET	Fluorescent sensor	pH = 3.0–7.4	4.4 (1) 4.6 (2) 4.8 (3)	/	Living cells	[79]

Table 2. *Cont.*

No.	Molecular Structure	Target	Sensing Mechanism	Sensor Type	Sensitive pH Range	pKa	Solution Systems	Application	Ref.
5		H+	FRET	Ratiometric sensor	pH = 4.0–8.0	7.1	/	Living cells	[80]
6		H+	FRET	Fluorescent and colorimetric sensor	/	/	DMF/H2O (v/v, 1:4) (pH = 7.2)	Living cells	[81]
7		H+	PET	Fluorescent and colorimetric sensor	pH = 1.0–7.5	2.59	THF/H2O (v/v, 1: 1)	/	[82]

Srivastava P., et al. reported a novel pH-responsive fluorescent sensor that consisted of three units (two phenanthrene and one rhodamine B), linked by click chemistry and possessed dual excitation and three color-emitting characteristics (Table 2, No. 7) [82]. Two phenanthrene units in the prepared structure provided more choices for signal response due to the abundant optical-spectral characteristics (Figure 39). The prepared sensor (pKa = 2.59 ± 0.04) showed a specific response in the pH range of 1.0 to 7.5 in THF-water mixtures in Britton-Robinson (B-R) buffer.
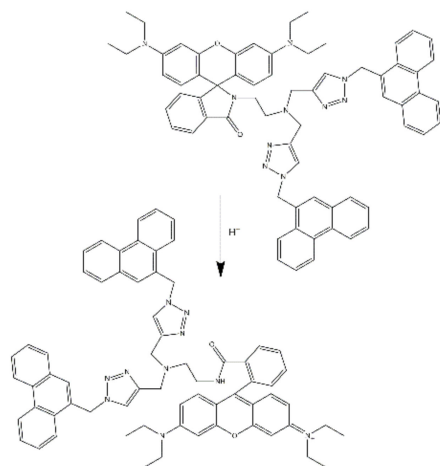

Figure 39. The possible sensing mechanism of the prepared sensor (Table 2, No. 7) for pH [82].
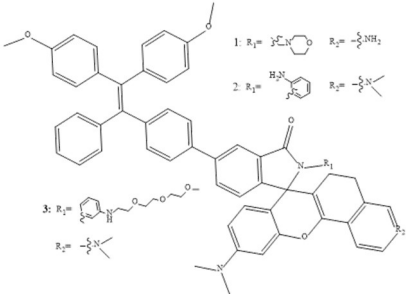
4. Rhodamine-Based Sensors for Anions and Others

Many small molecule indicators for cells or body state, such as H_2S, NO, and NADH, are playing a critical role in physiological and pathological processes including neuromodulation [83,84], apoptosis [85,86], and inflammation regulation [87–89]. There rhodamine derivatives sensors are also used for these indicator molecules, extending the application to biological systems.

Sensor No.1 [90] and No.2 (Table 3) [91] were used to detect NO over a wide pH range (4.0–12.0), designed with a characteristic cell membrane permeability for visualizing in vivo NO. Moreover, NO sensors are characterized by a high reaction rate due to their high chemical activity in short existence [90]. A selective and sensitive cationic fluorescent probe, named ROPD (Table 3, No. 1), was prepared by Wang Q., et al. [90] by grafting a NO-trapper o-phenylenediamine on a rhodamine fluorophore at the C-3 position through the Schiff base reaction. The presence of NO would block the PET of ROPD and induce fluorescence change (Figure 40). Sensor No. 2 (Table 3) was constructed from Rhodamine-B-en and 2-(pyridin-2-ylmethoxy) benzaldehyde by Alam R., et al. [91]. The presence of NO improved the formation of nitroso-hydroxylamine via the spirolactam ring opening mechanism (Figure 41). Resultantly, an obvious intensity enhancement in absorption and emission peaks was observed.
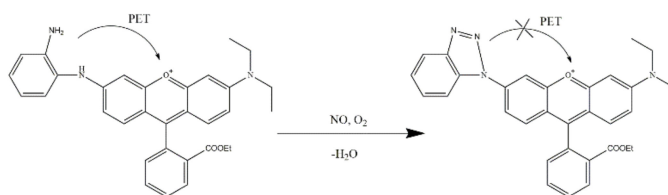
Figure 40. The proposed sensing mechanism of ROPD (Table 3, No. 1) for NO [90].

Table 3. Rhodamine-based sensors for anions and others.
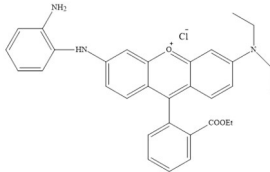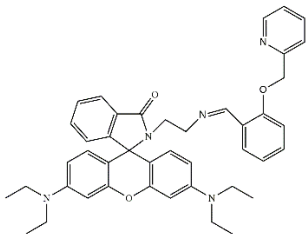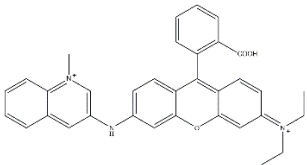
No.	Molecular Structure	Target	Probe Type	Sensing Mechanism	Sensor Type	Solution Systems	Application	Ref.
1		NO	Turn-on	PET blocked	Fluorescent probe	PBS buffers (pH = 7.4)	Living cells	[90]
2		NO	Turn-on	/	Fluorescent probe	HEPES buffers (pH = 7.4)	Living cells and zebrafish	[91]
3		NADH	Turn-on	/	Fluorescent probe	PBS buffers (pH = 7.4)	Living cells	[92]

Table 3. *Cont.*
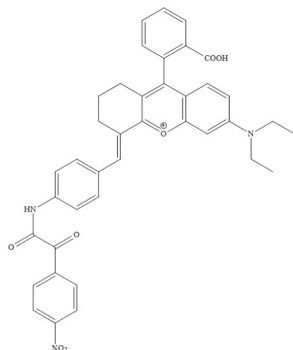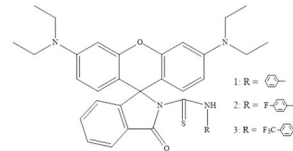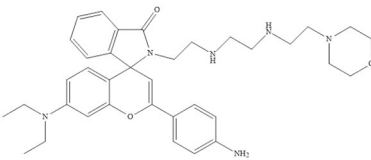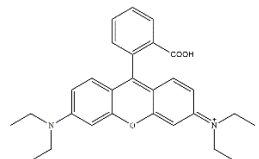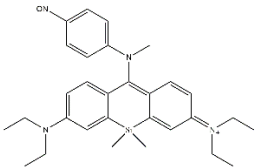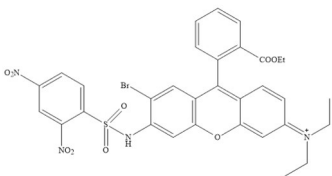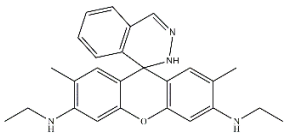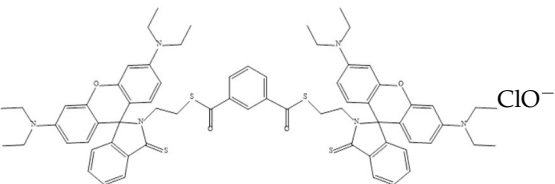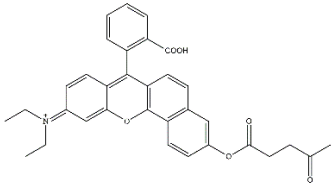
No.	Molecular Structure	Target	Probe Type	Sensing Mechanism	Sensor Type	Solution Systems	Application	Ref.
4		H$_2$O$_2$	Turn-on	PET blocked	Fluorescent sensor	PBS with 0.1% DMSO (pH = 7.4,)	Living cells	[93]
5		ATP	Turn-on	/	Fluorescent and colorimetric sensor	PBS solution (containing 40% DMSO)	Living cells	[94]
6		ATP	Turn-on	/	Fluorescent and colorimetric sensor	EtOH/ PBS buffer (1/99, *v/v*; pH = 7.4)	Living lysosomes	[95]
7		ACP	Turn-on	IFE	Fluorescent and colorimetric sensor	/	Human serum	[96]

Table 3. *Cont.*

No.	Molecular Structure	Target	Probe Type	Sensing Mechanism	Sensor Type	Solution Systems	Application	Ref.
8		Peroxynitrite (ONOO−)	Turn-on	PET blocked	Fluorescent probe	H2O/CH3CN (7:3, *v/v*) HEPES buffers (pH = 7.4)	Living cells	[97]
9		Thiophenols (-SH)	Turn-on	PET blocked	Fluorescent probe	DMSO/HEPES solution (1:1, *v/v*) (pH = 7.4)	Water and living cells	[98]
10		ClO−	Turn-on	/	Fluorescent and colorimetric sensor	C2H5OH/H2O (1:1, *v/v*)	Living lysosomes and real water samples	[99]
11		ClO−	Turn-on	/	Fluorescent and colorimetric sensor	CH3CH2OH-Tris (7/3, *v/v*, pH = 7.4)	Living cells	[100]
12		SO$_3^{2-}$	Turn-on	ICT	Fluorescent probe	PBS buffer (10 mM, pH 7.4, 1% DMSO)	Living cells and zebrafish	[101]
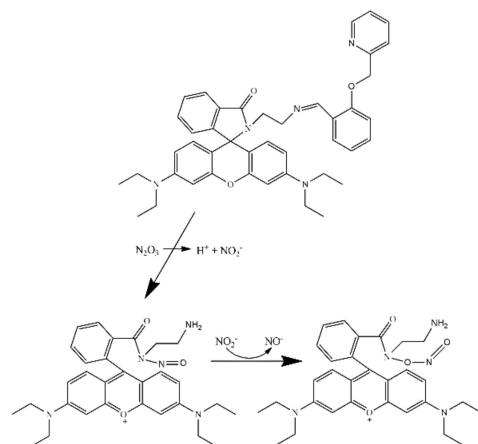
Figure 41. The proposed reaction mechanisms of the prepared sensor (Table 3, No. 2) with NO [91].

Rhodamine-based sensors designed for the detection of 4-dihydronicotinamide adenine dinucleotide (NADH), H_2O_2 (a kind of reactive oxygen species), and adenosine triphosphate (ATP) have gained significant attention in the bioimaging area. Sensor No.3 (Table 3) was synthesized via a redox-responsive 3-aminoquinoline appended rhodamine by Podder A., et al. This sensor was a sort of reaction type fluorescent sensor and showed a remarkably increasing fluorescent intensity in the presence of NADH [92]. Apart from the common detection function, the sensor (MQR) figured out the connection between NADH levels and metabolic abnormalities of high clinical significance (Figure 42).
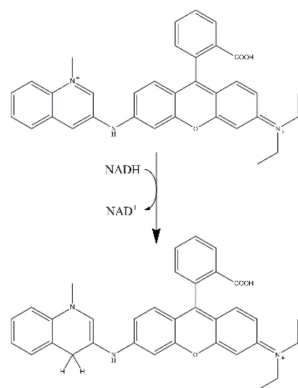
Figure 42. The possible sensing mechanism of MQR (Table 3, No. 3) for NADH [92].

Gu T., et al. reported another reaction type sensor, named RhB-NIR (Table 3, No.4), to detect the H_2O_2 in living cells [93]. This sensor was triggered by a classical Baeyer-Villiger reaction. Specifically, H_2O_2 attacked the carbonyl carbon of the amide bond in the sensor structure, causing the rearrangements of α-ketoamide groups (Figure 43). The formed intermediates were successively hydrolyzed, decarboxylated, and released into the fluorophore.
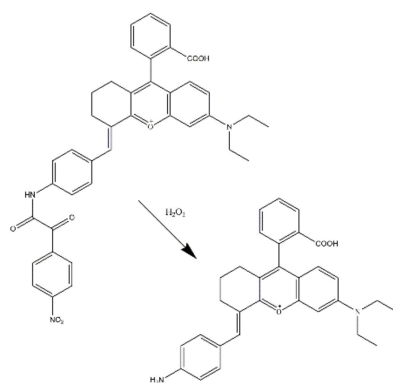
Figure 43. The proposed sensing mechanism of RhB-NIR (Table 3, No. 4) for H$_2$O$_2$ [93].

Sensor No.5 (Table 3) was also a kind of reaction-type sensor used for ATP detection [94] and Sensor No. 6 (Table 3) discriminated the ATP as hydrogen bonds formed between diethylenetriamine moiety of the sensor and phosphate groups of the target [95]. Three rhodamine derivatives (probes 1, 2, 3) were constructed by Liu Y. et al. (Table 3, No. 5) [94] and probe 2 demonstrated a specific target at mitochondrial and the real-time detection of ATP in living cells. Tikum A. F., et al. synthesized a NIR-fluorescent sensor (Table 3, No. 6), revealing a turn-on fluorescent response by changing the solution color (from colorless to purple) through the interaction with ATP (Figure 44) [95].
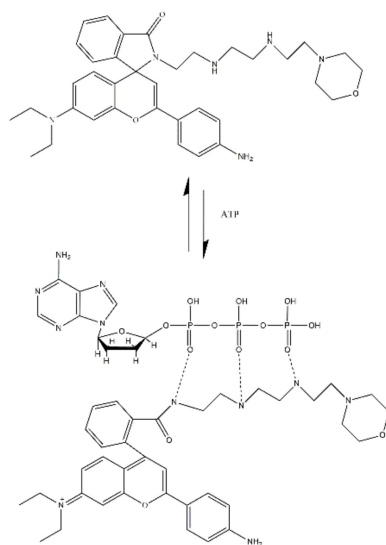
Figure 44. The proposed sensing mechanism of the prepared sensor (Table 3, No. 6) for ATP [95].

Apart from ATP, the rhodamine-based acid phosphatase (ACP)-detection sensor was reported based on the IFE between oxidized 3,3′,5,5′-tetramethylbenzidine (oxTMB), and rhodamine B [96]. Specifically, the fluorescence of rhodamine B was quenched by oxTMB, owing to spectral overlap between the emission of rhodamine B and the absorption of oxTMB. oxTMB was reduced by ascorbic acid, generated from ACP-inducing hydrolysis of 2-phospho-L-ascorbic acid trisodium salt. Thus, the internal filtering effect between rhodamine B and oxTMB was inhibited, realizing the determination of ACP.

Sensor Nos. 8–12 (Table 3) [97–101] were applied for anion detections. Among these, sensor No.8 (Table 3) was a Si-rhodamine-based sensor (SiNH) that showed a nanoscale response after capturing amphiphilic copolymers named mPEG-DSPE [97]. The amphiphilic mPEG-DSPE improved the water solubility of the prepared sensor which was applied to real-time analysis of endogenous ONOO$^-$ in living cells (Figure 45).
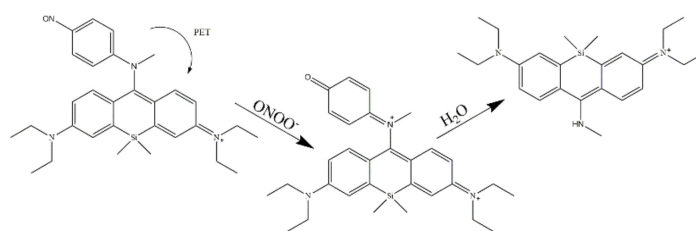
Figure 45. The proposed sensing mechanism of SiNH (Table 3, No. 8) [97].

Sensors for SH⁻ and ClO⁻ are useful in the environment and biosafety. SH⁻ is a highly toxic material and harmful to the environment, humans, and animals [102,103], and ClO− is a toxic disinfection by-product of hypochlorite salts [104], often used as a disinfectant in swimming pools and other water environments [105]. SH− sensor (Table 3 No. 9) [98] and ClO− sensors (Table 3 No. 10–11) [99,100] were applied to detect environment water samples and living cells, and both were convenient for monitoring human and animal health. Wu J., et al. chose the DNBS group as a cleavable quencher of rhodamine-based fluorescence since thiophenols removed the group and recovered the rhodamine fluorescence [98]. The sensing mechanism was attributed to the nucleophilic substitution reaction of thiophenols (Figure 46) and confirmed by HPLC.
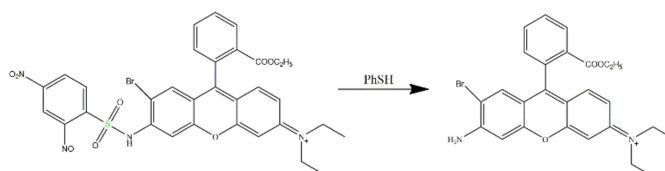
Figure 46. The proposed sensing mechanism of the prepared sensor (Table 3, No. 9) for PhSH [98].

Wang Z., et al. reported the rhodamine-based fluorescent sensor, named 6G-ClO (Table 3, No. 10), developed from 2-formyl rhodamine and used for ClO⁻ detection in water and HUVEC cells [99]. Apart from the application in ClO⁻-detection in water and living cells, a test strip was prepared with 6G-ClO and successfully used for semi-quantitative detection of the same molecule (Figure 47).
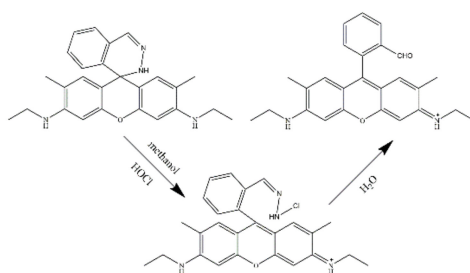
Figure 47. The proposed mechanism of 6G-ClO (Table 3, No. 10) with ClO⁻ [99].

Zhang D., et al. reported a ClO⁻ sensor (SRh) (Table 3, No. 11) synthesized by the conjugation of dual-binding benzene and rhodamine B [100]. SRh showed an "off-on" response to ClO⁻, visible to the naked eye (Figure 48). The detection limit was calculated to be 2.43×10^{-9} M. Wang K., et al. synthesized a turn-on NIR fluorescent sensor with rhodamine derivatives for SO_3^{2-} detection (Table 3, No. 12) [101]. The addition of SO_2^{3-} attacked the 4-position carbonyl group in levulinic acid and induced the ester bond cleavage, resulting in the formation of the fluorophore. The ICT process was then restored, and the sensor showed the corresponding NIR fluorescence (Figure 49).
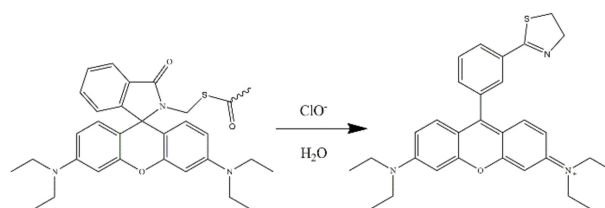
Figure 48. The proposed sensing mechanism of SRh (Table 3, No. 11) with ClO⁻ [100].
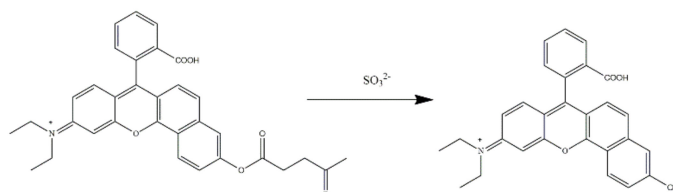
Figure 49. The possible reaction mechanism of the prepared sensor (Table 3, No. 12) for SO_3^{2-} [101].

5. Rhodamine-Based Sensors for Multi-Targets

Sensors No. 1, 2, and 3 (Table 4) were developed for the detection of both Hg^{2+} and Cu^{2+}. Chang L. L., et al. reported a Hg^{2+} and Cu^{2+}-responsive sensor, RhBH-HB-Ac, based on a completely different sensing mechanism in the absence and presence of UV irradiation (Table 4, No. 1) [106]. Without UV irradiation, this probe selectively recognized Hg^{2+} through colorimetric and fluorescent responses. Under UV irradiation, Cu^{2+} induced a significant color change in the sensor (Figure 50).
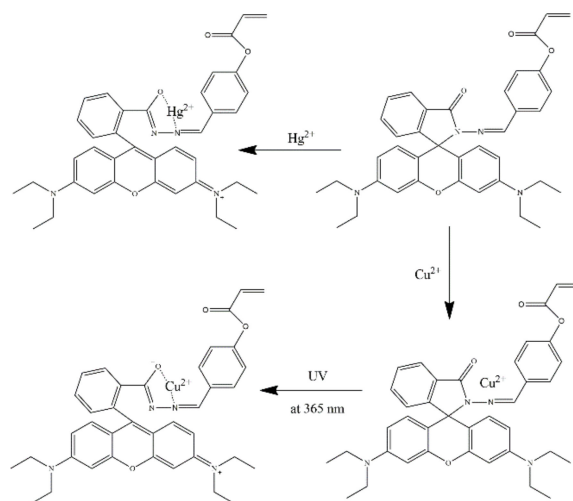
Figure 50. The sensing mechanism of RhBH-HB-Ac (Table 4, No. 1) [106].

Table 4. Rhodamine-based sensors for multi-targets.
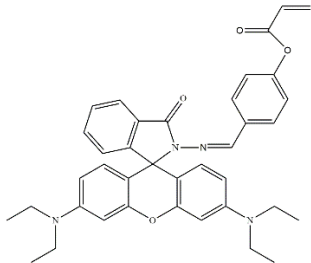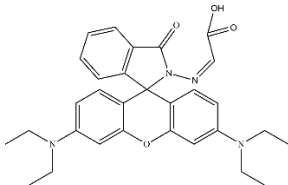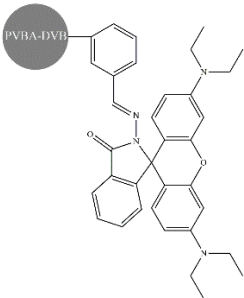
No.	Molecular Structure	Target	Sensing Mechanism	Sensor Type	LOD	Solution Systems	Application	Ref.
1		Hg^{2+} Cu^{2+}	/	Colorimetric and fluorescent probe	7.1×10^{-8} 1.5×10^{-7}	IPA/H_2O (8/1, *v/v*) (Iso-Propyl Alcohol)	/	[106]
2		Cu^{2+} Hg^{2+}	/	Fluorescent and colorimetric sensor	/	CH_3CN/ HEPES buffer (1/9, *v/v*; pH = 7.4)	/	[107]
3		Cu^{2+} Hg^{2+}	/	Fluorescent and colorimetric sensor	5.06×10^{-7} 3.90×10^{-7}	CH_3CN/H_2O (8/2, *v/v*) (pH = 7.2)	/	[108]
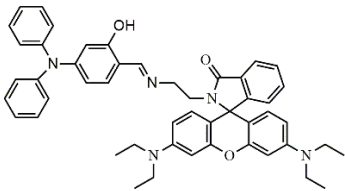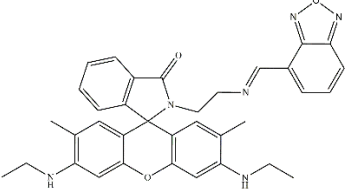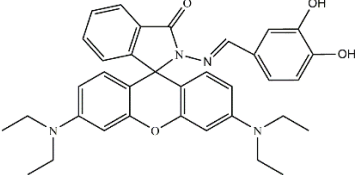
No.	Molecular Structure	Target	Sensing Mechanism	Sensor Type	LOD	Solution Systems	Application	Ref.
4		Hg^{2+} Al^{3+}	FRET	Fluorescent and colorimetric sensor	1.26×10^{-7} 1.9×10^{-7}	MeCN/H_2O (3/1, *v/v*) HEPES buffer (pH = 6.85)	/	[109]
5		Hg^{2+} Al^{3+}	FRET PET	Fluorescent probe	0.48×10^{-6} 7.18×10^{-8}	MeCN/H_2O (9/1, *v/v*)	Test paper	[110]
6		Hg^{2+} Al^{3+}	/	Fluorescent sensor	1.60×10^{-5} 6.54×10^{-6}	H_2O/EtOH (1:9, *v/v*) (pH = 7.4)	River water, paper test	[111]
7		Cu^{2+} Al^{3+}	/	Fluorescent and colorimetric sensor	9.90×10^{-9} 5.63×10^{-9}	MeCN/H_2O (6:4, *v/v*)	Living cells, natural mineral water, tap water	[112]

Table 4. *Cont.*
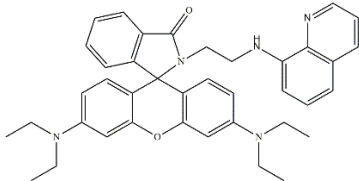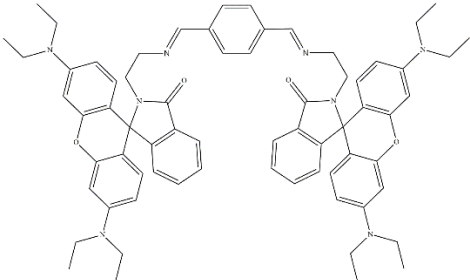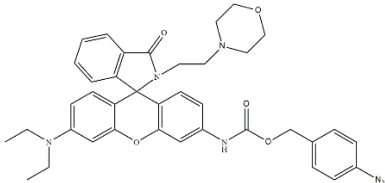
No.	Molecular Structure	Target	Sensing Mechanism	Sensor Type	LOD	Solution Systems	Application	Ref.
8		Cr^{3+} Cu^{2+}	/	Colorimetric sensor	4.7×10^{-8} 7.6×10^{-8}	CH_3CN solution Ethanol solution	/	[113]
9		Al^{3+} CN^-	PET blocked	Fluorescent and colorimetric sensor	1.68×10^{-9} 0.82×10^{-9}	HEPES buffer (pH = 7.04)	Living cells	[114]
10		H^+ H_2S	ICT (Intramolecular charge transfer)	Fluorescent probe		/	Living cells	[115]

Table 4. *Cont.*
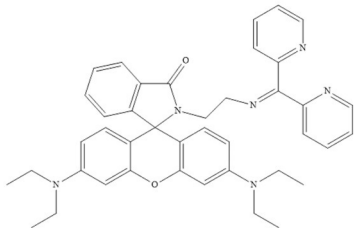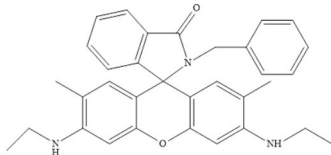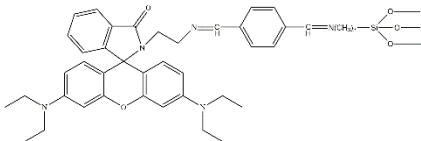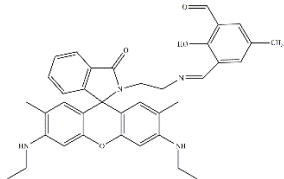
No.	Molecular Structure	Target	Sensing Mechanism	Sensor Type	LOD	Solution Systems	Application	Ref.
11		Cr^{3+} Al^{3+} Fe^{3+}	/	Fluorescent and colorimetric sensor	3.16×10^{-9} 1.17×10^{-9} 2.50×10^{-9}	H_2O/EtOH (1/1, *v/v*)	/	[116]
12		Cr^{3+} Al^{3+} Fe^{3+}	/	Colorimetric sensor	2.28×10^{-6} 1.28×10^{-6} 1.34×10^{-6}	H_2O/CH_3CN (4/1, *v/v*, pH = 7.2)	Living cells	[117]
13		Cr^{3+} Al^{3+} Fe^{3+}	/	Fluorescent and colorimetric sensor	9.18×10^{-9} 5.40×10^{-9} 7.23×10^{-7}	H_2O/EtOH (14/1, *v/v*)	/	[118]
14		Cr^{3+} Al^{3+} Fe^{3+}	/	Fluorescent and colorimetric sensor	1.58×10^{-8} 6.97×10^{-9} 1.4×10^{-8}	CH_3OH/H_2O (9/1, *v/v*) HEPES buffer (pH = 7.4)	Living cells	[119]

Table 4. *Cont.*

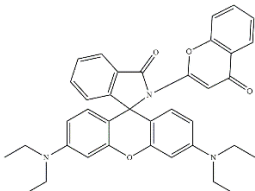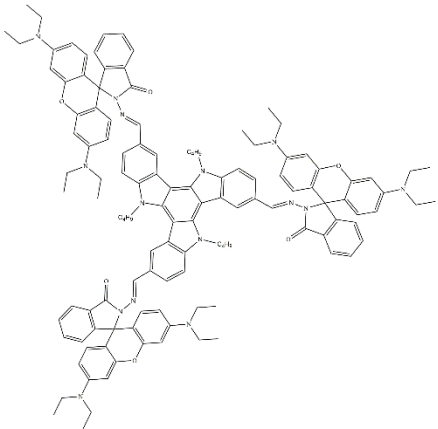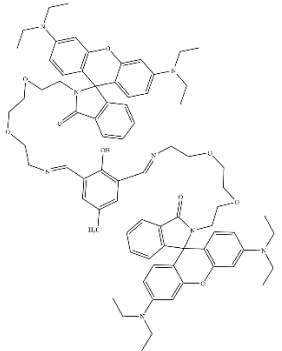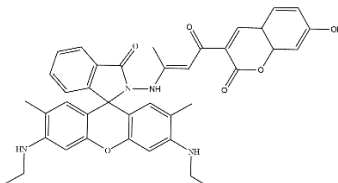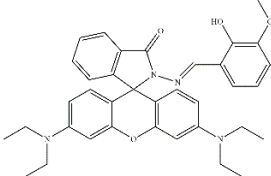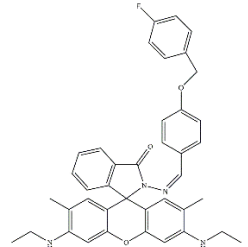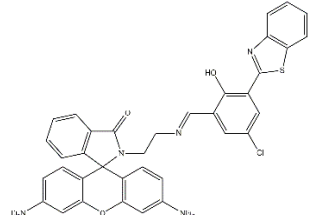| No.	Molecular Structure	Target	Sensing Mechanism	Sensor Type	LOD	Solution Systems	Application	Ref.
15		Cr^{3+} Al^{3+} Fe^{3+}	TBET	Ratiometric fluorescent and colorimetric sensor	1.70×10^{-4} 2.3×10^{-5} 2.5×10^{-5}	MeOH	Test strips	[120]
16		Zn^{2+} Cd^{2+} Hg^{2+}	PET-CHEF PET-CHEF PET-FRET	Fluorescent and colorimetric sensor	1.2×10^{-9} 9.6×10^{-9} 1.5×10^{-10}	MeOH/H_2O, (4/1, *v/v*) HEPES buffer (pH = 7.4)	Sea fish and water samples	[121]

Table 4. *Cont.*

No.	Molecular Structure	Target	Sensing Mechanism	Sensor Type	LOD	Solution Systems	Application	Ref.
17		Cu^{2+} Co^{2+} Al^{3+}	/	Fluorescent sensor	8.68×10^{-8} / 1.06×10^{-9}	CH_3OH CH_3OH/H_2O H_2O	Living cells	[122]
18		Cu^{2+} Ni^{2+} Co^{2+}	/	Colorimetric sensor	4.0×10^{-8} 3.2×10^{-7} 4.8×10^{-7}	DMSO/TN (2:1, *v/v*) (pH = 7.5)	Test strips	[123]
19		Al^{3+} Ga^{3+} In^{3+} Tl^{3+}	/	Fluorescent and colorimetric sensor	2.66×10^{-8} 1.04×10^{-7} 8.19×10^{-8} 3.10×10^{-8}	10 mM HEPES buffer (pH = 7.4) in water/ethanol (1:9, *v/v*)	River water	[124]
20		Al^{3+} Cu^{2+} Hg^{2+} S^{2-} CN^{-}	ICT	Fluorescent and colorimetric sensor	2.1×10^{-7} 3.2×10^{-7} 4.0×10^{-7} / /	CH3CN (5.0×10^{-5} mol/L)	Logic gate	[125]

Wang K., et al. designed a novel bifunctional rhodamine-based sensor, comprising hydrazide and formylformic acid (Table 4, No. 2) [107]. The prepared sensor was used for differential detection of Cu^{2+} and Hg^{2+} by different sensing assays in CH_3CN-HEPES buffer solution (20 mM, pH 7.4) (1:9, *v/v*). A colorimetric change in the presence of Cu^{2+} was observed along with the fluorescent enhancement due to the coordination-induced spirolatam-ring opening process (Figure 51).
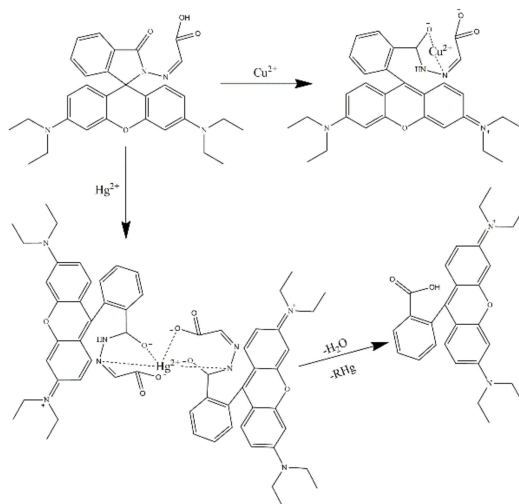
Figure 51. Proposed binding modes of the prepared sensor (Table 4, No. 2) with Cu^{2+} and Hg^{2+} [107].

RHB (Table 4, No. 3) was a reusable spherical solid supported sensor prepared by a simple two-step route. (1) synthesis of aldehyde functional spherical crosslinked poly(vinylbenzaldehyde-co-divinylbenzene) microbeads (PVBA-DVB) via precipitation polymerization and (2) attaching the rhodamine hydrazide to aldehyde groups via imine linkages [108]. The prepared RHB sensor displayed selective turn-on fluorescence and colorimetric response to Cu^{2+} and Hg^{2+} (Figure 52).
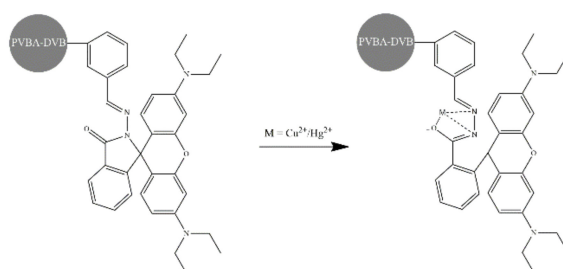
Figure 52. The proposed sensing mechanism of RHB (Table 4, No. 3) to Cu^{2+} and Hg^{2+} [108].

Sensor No. 4, 5, and 6 (Table 4) were developed for the co-detection of Al^{3+} and Hg^{2+}. Among these, sensor No. 4 was a chromenone-based rhodamine, synthesized by Mondal S., et al. [109], and was used for fluorometric and colorimetric recognition of Al^{3+} and Hg^{2+} in $CH_3CN:H_2O$ (3:1, *v/v*, 10 mM HEPES buffer, pH = 6.85). In addition, the recognition of Al^{3+} and Hg^{2+} was discriminated by adding the tetrabutylammonium iodide salts. In the presence of I^-, the color change was completely discharged, induced by Hg^{2+}, and color was retained by Al^{3+} (Figure 53). Sensor TR (Table 4, No.5), was a rhodamine-based sensor appended with triphenylamine and developed for Al^{3+} and Hg^{2+} detection with different sensing mechanisms (Figure 54) [110]. Furthermore, TR-coated test papers were successively prepared for the rapid detection of Al^{3+} and Hg^{2+}.
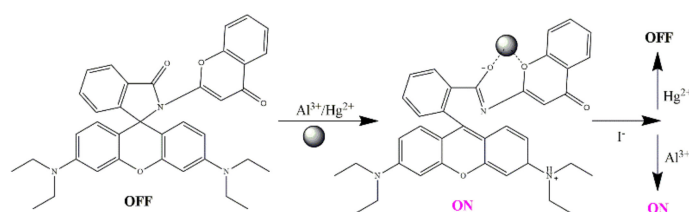
Figure 53. The sensing mechanism of the prepared sensor (Table 4, No. 4) for Al^{3+} and Hg^{2+} [109].
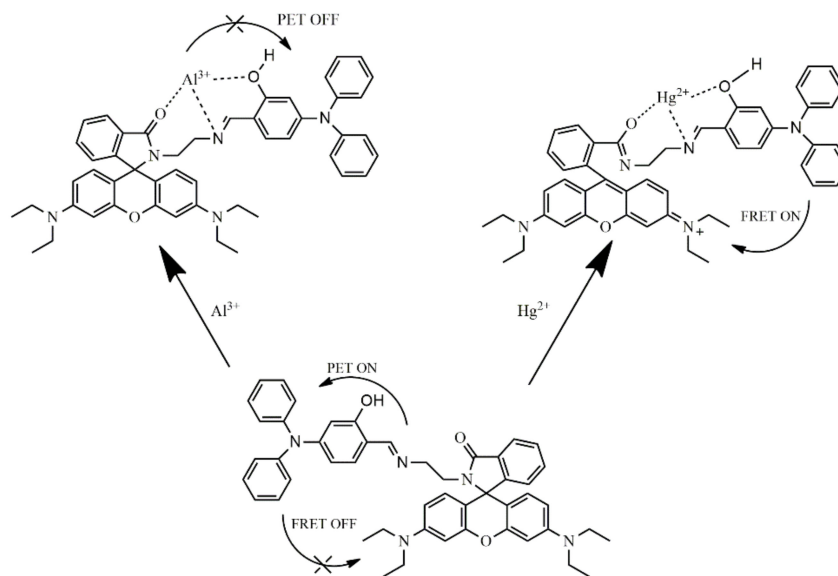
Figure 54. Proposed sensing mechanism of TR (Table 4, No. 5) for Al^{3+} and Hg^{2+} [110].

Hazra A., et al. synthesized a rhodamine-based sensor, named RBO (Table 4, No. 6) through the reaction of N-(rhodamine-6G)lactam-ethylenediamine and 2,1,3-benzoxadiazole-4-carbaldehyde [111] and used for selective detection of Al^{3+} and Hg^{2+} in 10 mM HEPES buffer in water: ethanol (1:9, pH = 7.4) (Figure 55). Furthermore, the induced response by Al^{3+} and Hg^{2+} was recovered with the assistance of fluoride or sulfide ions, thus opening a path for the construction of logic gates.
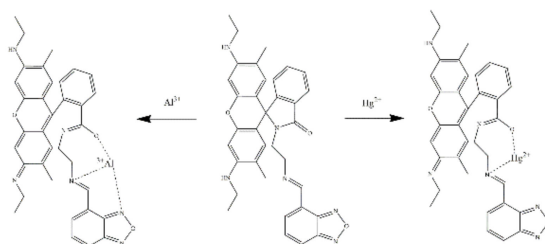
Figure 55. The possible sensing mechanism of RBO (Table 4, No. 6) for Al^{3+} and Hg^{2+} [111].

Chan W. C., et al. reported a novel rhodamine-based sensor, R34 (Table 4, No. 7), synthesized by the reaction of rhodamine B hydrazide and 3,4- dihydroxybenzaldehyde [112]. R34 exhibited a sensitive and selective response to Al^{3+} and Cu^{2+} and displayed significant color change from colorless to pink and colorless to orange for Al^{3+} and Cu^{2+}, respectively (Figure 56). The prepared sensor was successfully used in actual water samples and living cells bio-imaging.
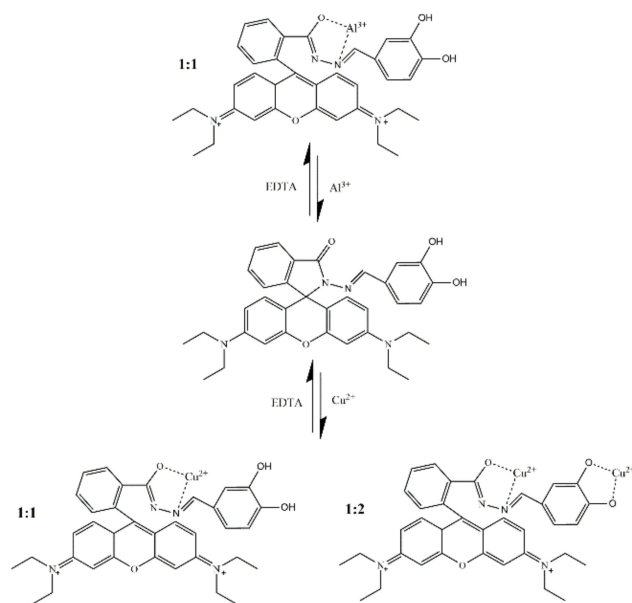
Figure 56. The proposed mechanism for interaction between R34 (Table 4, No. 7) and Al^{3+}/Cu^{2+} [112].

Zhang Z., et al. reported a rhodamine-based sensor with solvent-dependent binding properties for differential detection of Cr^{3+} and Cu^{2+} (Table 4, No. 8) [113]. The sensor depicted a turn-on fluorescence response with high selectivity and sensitivity to Cr^{3+} and Cu^{2+} in acetonitrile and ethanol solution, respectively (Figure 57). In acetonitrile medium, the acquired sensor showed different colorimetric, providing easy and differential analysis of Cr^{3+} and Cu^{2+} through naked eyes.
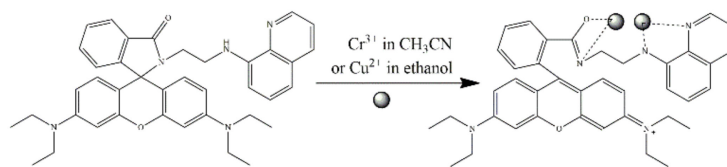
Figure 57. The sensing mechanism of this prepared sensor (Table 4, No. 8) for Cr^{3+} and Cu^{2+} [113].

A sensor, with a dual function of distinguishing Al^{3+} and CN^{-}, named sensor No.9 in Table 4 [114], showed strong fluorescence and pink color for Al^{3+}, specifically recognizing CN^{-} with a detection limit of 0.815×10^{-8} M accompanied by reduced fluorescence intensity. The possible binding mechanism of the prepared sensor with Al^{3+} and CN^{-} is shown in Figure 58.

A rhodamine-based sensor, MF-N$_3$ (Table 4, No. 10), was reported by Zhu L., et al. to selectively accumulate in lysosomes and show turn-on fluorescence for both H$_2$S and H$^+$ [115]. Owing to ingenious molecular design, MF-N$_3$ exhibited strong fluorescence with H$_2$S only in acid conditions, since endogenous H$_2$S is mainly produced in cells with pH in the acidic range. This sensor containing the spirolactam group was modified with 4-azidobenzyl carbamate that reacted with H$_2$S and then transformed to amine, enabling strong fluorescence (Figure 59).
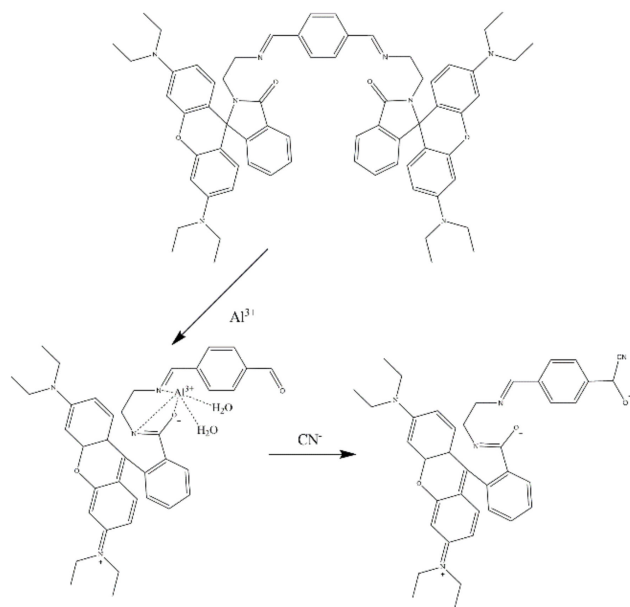
Figure 58. The possible binding mechanism of the prepared sensor (Table 4, No. 9) for Al^{3+} and CN^- [114].
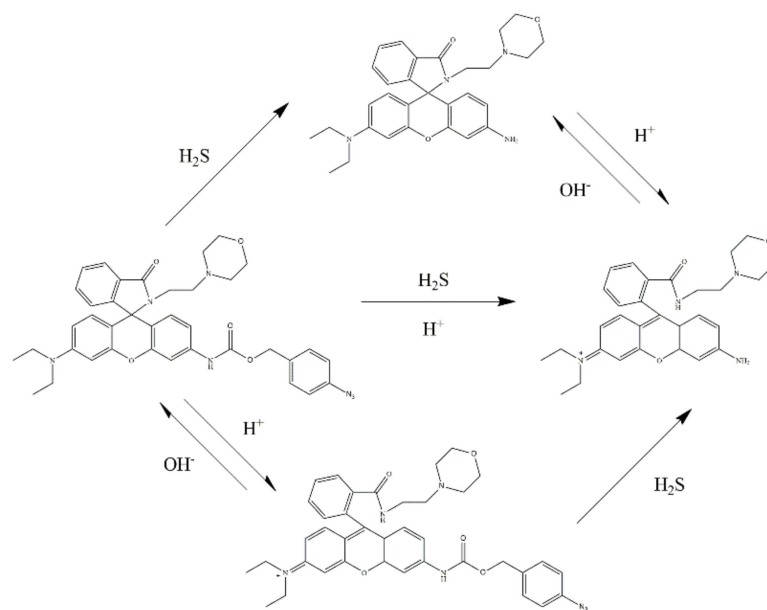
Figure 59. The sensing mechanism of MF-N$_3$ (Table 4, No. 10) for dual-response to H_2S and protons [115].

Five rhodamine-based sensors (Table 4, No. 11–15) were designed with distinctive characters for the detection of trivalent metal ions, such as Fe^{3+}, Cr^{3+}, and Al^{3+}. Among these, sensor No.11 (RDP), reported by Kilic H. and Bozkurt E., possessed the best selectivity and the lowest detection limit (2.50×10^{-9} M, 3.16×10^{-9} M, and 1.17×10^{-9} M for Fe^{3+}, Cr^{3+} and Al^{3+}, respectively). The interaction ratio between the prepared RDP and target ions was 1:2. Similarly, sensor No. 12 (Table 4) was a rhodamine 6G-benzylamine, synthesized by Das D., et al. [117]. The prepared sensor exhibited crystal structure due to only hydrocarbon skeletons in the extended part. In the presence of Fe^{3+}, Cr^{3+}, and Al^{3+}, the sensor showed large enhancements in fluorescence intensity, thus, realizing bio-imaging in living cells.

Sensor No. 13 (Table 4), named RFMS, was constructed by rhodamine 6G functionalized mesoporous silica and served to recognize the target ions and remove them from the matrix [118]. The prepared RFMS had no absorption band in the visible region and possessed low fluorescence at 550 nm. In the presence of Fe^{3+}, Cr^{3+}, and Al^{3+}, RFMS exhibited an absorption band at around 528 nm and the intensity was also enhanced (Figure 60). The opening of the spirolactam ring, induced by the interactions with Fe^{3+}, Cr^{3+}, and Al^{3+}, resulted in a visible color change of RFMS solution from colorless to pink. The removal efficiency of RFMS for Fe^{3+}, Cr^{3+}, and Al^{3+} was up to 90%.
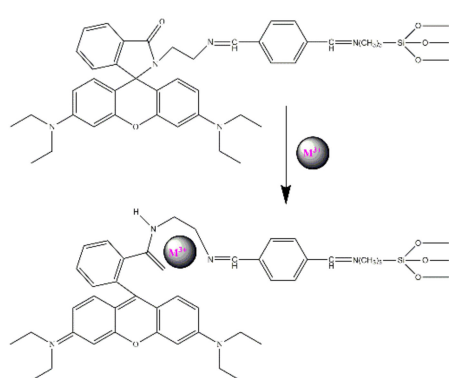
Figure 60. The possible sensing mechanism of RFMS (Table 4, No. 13) to Fe^{3+}, Cr^{3+} and Al^{3+} [118].

Roy A., et al. reported a rhodamine-based chemosensor, HL-CHO (Table 4, No. 14) for Fe^{3+}, Cr^{3+}, and Al^{3+} ions [119]. The fluorescence intensity of HL-CHO in HEPES buffer in methanol: water (9: 1, *v/v*) (pH 7.4) at 550 nm increased by 800, 588, and 1466 for Fe^{3+}, Cr^{3+}, and Al^{3+}, respectively (Figure 61). Sensor No. 15 (Table 4), TAT-ROD was reported by Sadak A. E. and Karakuş E., showing high sensitivity and selectivity to Fe^{3+}, Cr^{3+}, and Al^{3+} via TBET pathway. The TAT-ROD enabled Fe^{3+}, Cr^{3+}, and Al^{3+} recovery in the presence of ethylenediaminetetraacetic acid (EDTA), as shown in Figure 62. Banerjee M., et al. reported a multi-signaling rhodamine-based sensor for rapid recognition of Zn^{2+}, Cd^{2+}, and Hg^{2+} (Table 4, No. 16) [121]. The prepared sensor displayed a specific response to Zn^{2+}, Cd^{2+}, and Hg^{2+} via PET-CHEF-FRET processes and was applied to detect Zn^{2+}, Cd^{2+}, and Hg^{2+} in sea fish and water samples.
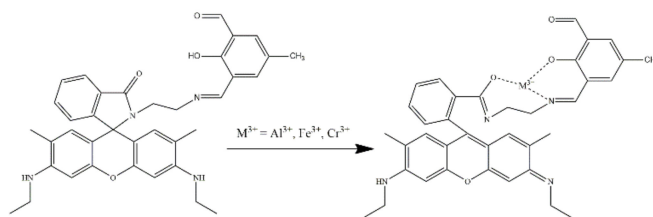
Figure 61. The proposed sensing mechanism of HL-CHO to Fe^{3+}, Cr^{3+} and Al^{3+} [119].
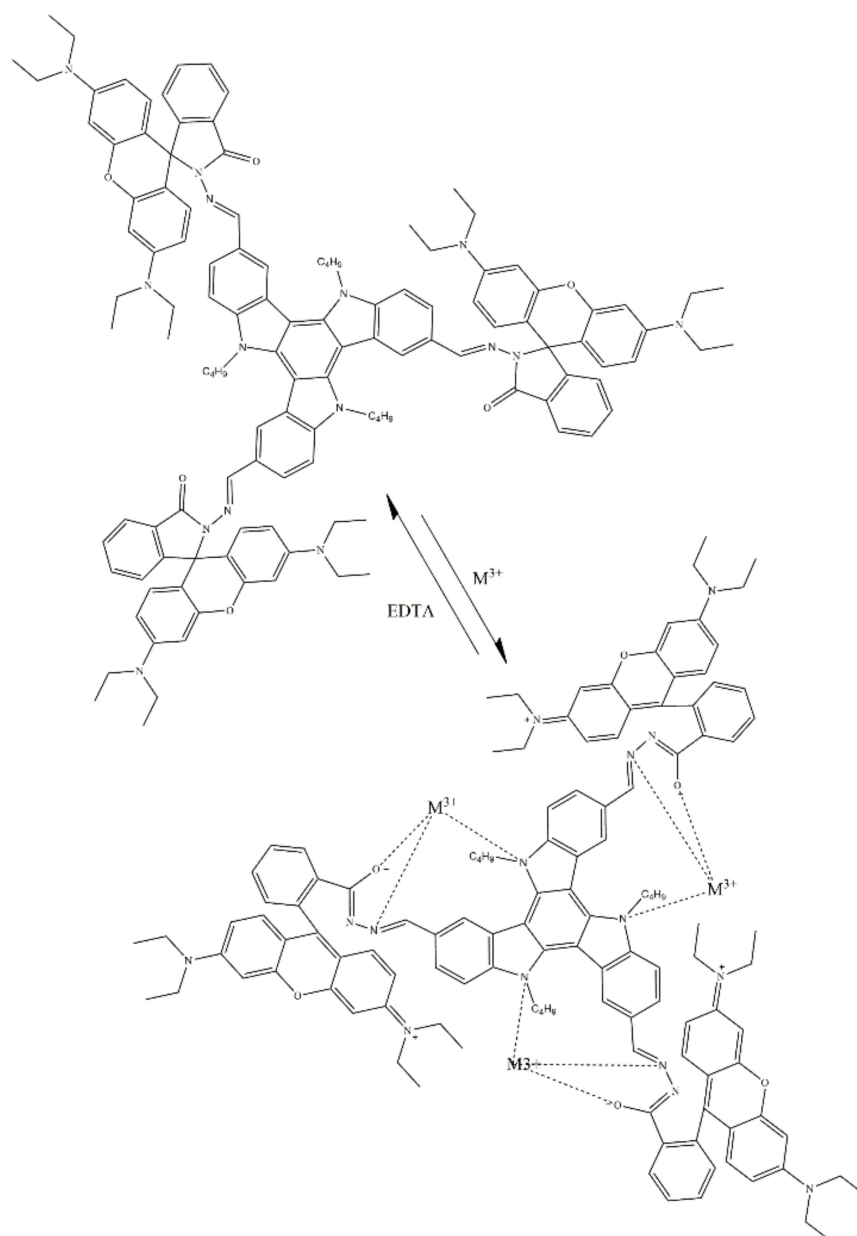
Figure 62. The proposed binding mechanism of TAT-ROD (Table 4, No. 15) to Fe^{3+}, Cr^{3+} and Al^{3+} [120].

Wang Y., et al. designed a rhodamine hydrazone (Table 4, No. 17), displaying exceptional selectivity to Cu^{2+}, Co^{2+}, and Al^{3+} (Figure 63) [122]. The prepared sensor exhibited fluorescence enhancement in methanol solution when Co^{2+} was added to the solution and showed a specific response to Al^{3+} in nearly pure water media. For Cu^{2+}, the acquired sensor demonstrated a color change response in methanol or water solutions.
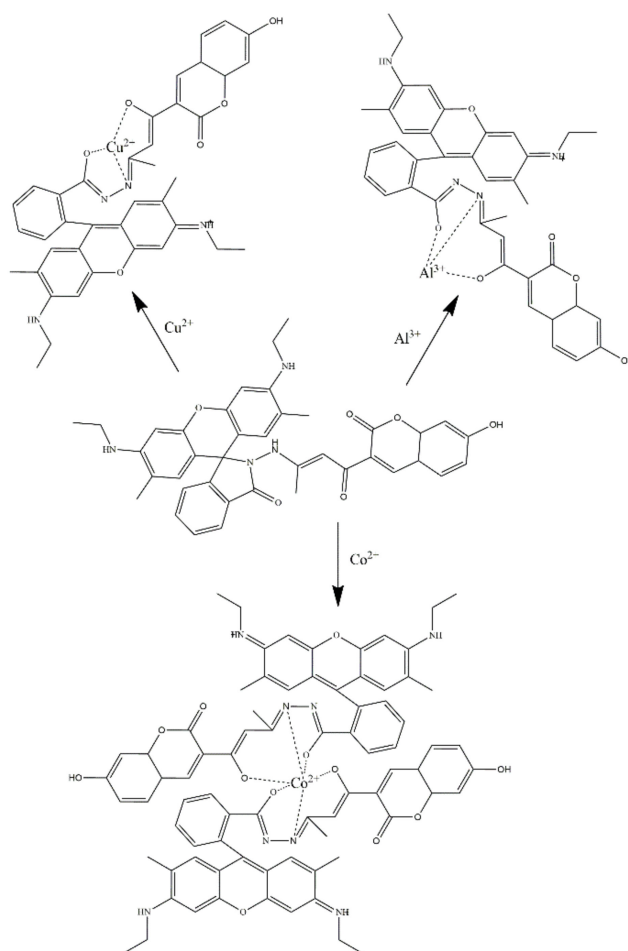
Figure 63. The proposed reaction mechanism of the prepared sensor (Table 4, No.17) with Cu^{2+}, Co^{2+}, and Al^{3+} [122].

Pungut N. A. S., et al. reported a colorimetric sensor (RBOV) that displayed a sensitive and selective response to Cu^{2+}, Ni^{2+}, and Co^{2+} in an aqueous medium (Table 4, No. 18) [123]. The detection limits for three metal ions were 4.0×10^{-8} M, 3.2×10^{-7} M, and 4.8×10^{-7} M, respectively. The sensing mechanism of RBOV for Cu^{2+}, Ni^{2+}, and Co^{2+} was analyzed, demonstrating a 1:1 stoichiometry of sensor-metal complex for all target ions. Hazra A. and Roy P. synthesized a new rhodamine-based sensor (Table 4, No. 19) for the colorimetric and fluorescence detection of group 13 cations (Al^{3+}, Ga^{3+}, In^{3+}, and Tl^{3+}) in 10 mM HEPES buffer (pH = 7.4) in water/ethanol (1:9, *v/v*) [124]. The prepared sensor demonstrated fluorescence enhancement and color change because of spirocyclic ring opening induced by the target ions (Figure 64).
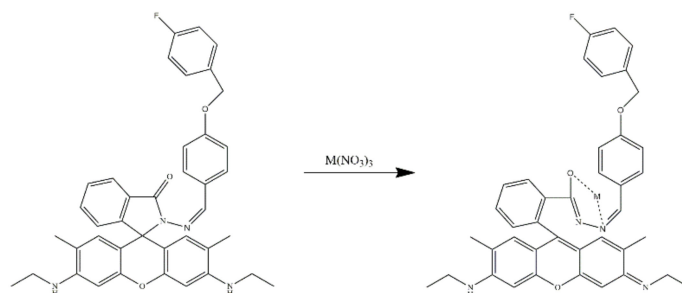
Figure 64. The possible sensing mechanism of the prepared sensor (Table 4, No.19) to Al^{3+}, Ga^{3+}, In^{3+} and Tl^{3+} [124].

Podshibyakin V. A., et al. reported a solvent-dependent multifunctional rhodamine-based sensor for visible selective detection of Al^{3+}, Cu^{2+}, Hg^{2+}, S^{2-} and CN^- (Table 4, No. 20) [125]. This prepared sensor showed selectivity to Al^{3+} in ethanol. The complexes of the sensor and Cu^{2+} and Hg^{2+} were used to detect S^{2-} and CN^-, respectively (Figure 65).
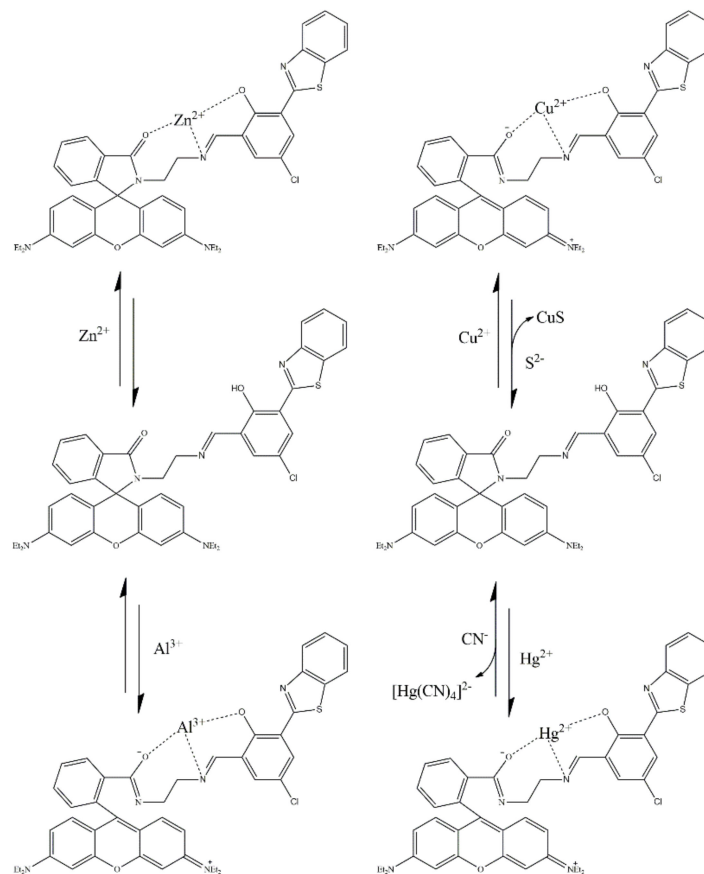
Figure 65. The proposed mechanism of coordination between the prepared sensor (Table 4, No. 20) and the target ions [125].

6. Conclusions and Perspective

Rhodamine and its derivatives possess excellent optical properties: good photo-irradiation stability, high fluorescence quantum yield, and so on. Chemosensors based on rhodamine and its derivatives have attracted extensive attention in areas of chemistry material, biology, medical, and health care. These sensors play an important role as simple, fast, economic, and efficient tools for monitoring environmental quality, health, and mechanism of physiological activity disorder. The unique and convenient close-open ring structure of rhodamine derivatives before and after the addition target induce color and fluorescent changes, showing great benefit for obviously detecting target analyte. Moreover, the fine biocompatibility and near-infrared fluorescence of rhodamine derivatives make them an excellent choice for bio-sensor construction. This review has summarized the development and achievements of rhodamine-based sensors in the past four years and found that there are still spaces for improvements in sensor design and synthesis. The review is intended to bring new clues or bright ideas for further advances in rhodamine-based chemosensors.

The Schiff base reaction is the most common synthesis mechanism when designing rhodamine-based sensors. Other reactions, such as the Mannich reaction, and the Baeyer-Villiger reaction, could be considered in the future. As for the sensing mechanism, coordination between the sensor and target ions is the most common and the coordination atoms are mainly N, O, and S. Other sensing mechanisms, such as reaction-type sensing, especially reversible reaction-type sensing mechanisms, are also attractive choices.

For sensitivity and selectivity, the coordination groups containing electron-rich structures such as carbon-oxygen double bonds. Carbon-nitrogen double bonds are the primary choice when designing the sensors. Apart for sensitivity and selectivity, water solubility is the most significant property of rhodamine-based sensors, concerning the applications in environmental samples. Besides, cell membrane-permeability, cytotoxicity, and organelle localization are all necessary factors that should be taken into consideration in biological applications. In addition, probes based on fluorophore with NIR fluorescence are better due to their anti-interference capability.

As for the rhodamine-based sensor for multi-targets, there are a few strategies for selective recognition; for example, the "multi recognition group" strategy, and the "solvent-dependent sensing" strategy. The former is more reported whereas the latter is superior in sensing performance due to the advantage of interference elimination. Thus, the rhodamine-based sensors for multi-targets via the "solvent-dependent sensing" strategy need to be further developed.

References

1. Kaur, B.; Kaur, N.; Kumar, S. Colorimetric metal ion sensors—A comprehensive review of the years 2011–2016. *Coord. Chem. Rev.* **2018**, *358*, 13–69. [CrossRef]
2. Park, S.-H.; Kwon, N.; Lee, J.-H.; Yoon, J.; Shin, I. Synthetic ratiometric fluorescent probes for detection of ions. *Chem. Soc. Rev.* **2020**, *49*, 143–179. [CrossRef] [PubMed]
3. Shree, G.J.; Sivaraman, G.; Siva, A.; Chellappa, D. Anthracene-and pyrene-bearing imidazoles as turn-on fluorescent chemosensor for aluminum ion in living cells. *Dye. Pigment.* **2019**, *163*, 204–212. [CrossRef]
4. Wu, D.; Sedgwick, A.C.; Gunnlaugsson, T.; Akkaya, E.U.; Yoon, J.; James, T.D. Fluorescent chemosensors: The past, present and future. *Chem. Soc. Rev.* **2017**, *46*, 7105–7123. [CrossRef] [PubMed]
5. Rasheed, T.; Li, C.; Bilal, M.; Yu, C.; Iqbal, H.M.N. Potentially toxic elements and environmentally-related pollutants recognition using colorimetric and ratiometric fluorescent probes. *Sci. Total Environ.* **2018**, *640*, 174–193. [CrossRef] [PubMed]
6. Chen, S.-H.; Jiang, K.; Xiao, Y.; Cao, X.-Y.; Arulkumar, M.; Wang, Z.-Y. Recent endeavors on design, synthesis, fluorescence mechanisms and applications of benzazole-based molecular probes toward miscellaneous species. *Dye. Pigment.* **2020**, *175*, 108157. [CrossRef]
7. Kwon, N.; Hu, Y.; Yoon, J. Fluorescent Chemosensors for Various Analytes Including Reactive Oxygen Species, Biothiol, Metal Ions, and Toxic Gases. *ACS Omega* **2018**, *3*, 13731–13751. [CrossRef]
8. Wu, D.; Chen, L.; Xu, Q.; Chen, X.; Yoon, J. Design Principles, Sensing Mechanisms, and Applications of Highly Specific Fluorescent Probes for HOCl/OCl(). *Acc. Chem. Res.* **2019**, *52*, 2158–2168. [CrossRef]
9. State Administration for Market Regulation; National Standardization Administration. *GB 5749-2022*; Standards for Drinking Water Quality: National Standards of the People's Republic of China. National Health Commission of the People's Republic of China: Beijing, China, 2022.
10. Han, B.; Hu, X.; Yan, Q.; Jiang, J.; He, G. Ag-location-based color-tunable fluorescent AuAg nanoclusters for "turn-on" and "turn-off" detection of l-cysteine. *Sens. Actuators B Chem.* **2019**, *284*, 695–703. [CrossRef]
11. Tan, X.; Liu, S.; Shen, Y.; He, Y.; Yang, J. Quantum dots (QDs) based fluorescence probe for the sensitive determination of kaempferol. *Spectrochim. Acta Part A Mol. Biomol. Spectrosc.* **2014**, *133*, 66–72. [CrossRef]
12. Vikrant, K.; Kumar, V.; Ok, Y.S.; Kim, K.-H.; Deep, A. Metal-organic framework (MOF)-based advanced sensing platforms for the detection of hydrogen sulfide. *TrAC Trends Anal. Chem.* **2018**, *105*, 263–281. [CrossRef]
13. Li, Z.; Zhi, Y.; Shao, P.; Xia, H.; Li, G.; Feng, X.; Chen, X.; Shi, Z.; Liu, X. Covalent organic framework as an efficient, metal-free, heterogeneous photocatalyst for organic transformations under visible light. *Appl. Catal. B Environ.* **2019**, *245*, 334–342. [CrossRef]
14. Chen, H.; Lin, W.; Jiang, W.; Dong, B.; Cui, H.; Tang, Y. Locked-flavylium fluorescent dyes with tunable emission wavelengths based on intramolecular charge transfer for multi-color ratiometric fluorescence imaging. *Chem. Commun.* **2015**, *51*, 6968–6971. [CrossRef] [PubMed]
15. Dsouza, R.N.; Pischel, U.; Nau, W.M. Fluorescent Dyes and Their Supramolecular Host/Guest Complexes with Macrocycles in Aqueous Solution. *Chem. Rev.* **2011**, *111*, 7941–7980. [CrossRef] [PubMed]
16. Noelting, E.; Dziewonsky, K. Ber. Dtsch. *Chem. Ges* **1905**, *38*, 3516. [CrossRef]

17. Kim, H.N.; Lee, M.H.; Kim, H.J.; Kim, J.S.; Yoon, J. A new trend in rhodamine-based chemosensors: Application of spirolactam ring-opening to sensing ions. *Chem. Soc. Rev.* **2008**, *37*, 1465–1472. [CrossRef]

18. Dujols, V.; Ford, F.; Czarnik, A.W. A long-wavelength fluorescent chemodosimeter selective for Cu (II) ion in water. *J. Am. Chem. Soc.* **1997**, *119*, 7386–7387. [CrossRef]

19. Yang, Y.-K.; Yook, K.-J.; Tae, J. A rhodamine-based fluorescent and colorimetric chemodosimeter for the rapid detection of Hg2+ ions in aqueous media. *J. Am. Chem. Soc.* **2005**, *127*, 16760–16761. [CrossRef]

20. Chen, G.; Guo, Z.; Zeng, G.; Tang, L. Fluorescent and colorimetric sensors for environmental mercury detection. *Analist* **2015**, *140*, 5400–5443. [CrossRef]

21. Roy, P. Recent advances in the development of fluorescent chemosensors for Al(3). *Dalton Trans.* **2021**, *50*, 7156–7165. [CrossRef]

22. Jain, N.; Kaur, N. A comprehensive compendium of literature of 1,8-Naphthalimide based chemosensors from 2017 to 2021. *Coord. Chem. Rev.* **2022**, *459*, 214454. [CrossRef]

23. Zhu, H.; Liu, C.; Su, M.; Rong, X.; Zhang, Y.; Wang, X.; Wang, K.; Li, X.; Yu, Y.; Zhang, X.; et al. Recent advances in 4-hydroxy-1,8-naphthalimide-based small-molecule fluorescent probes. *Coord. Chem. Rev.* **2021**, *448*, 214153. [CrossRef]

24. Zhang, J.; Zhu, M.; Jiang, D.; Zhang, H.; Li, L.; Zhang, G.; Wang, Y.; Feng, C.; Zhao, H. A FRET-based colorimetric and ratiometric fluorescent probe for the detection of Cu^{2+} with a new trimethylindolin fluorophore. *New J. Chem.* **2019**, *43*, 10176–10182. [CrossRef]

25. Chen, H.; Jin, X.; Zhang, W.; Lu, H.; Shen, W. A new rhodamine B-based 'off-on' colorimetric chemosensor for Pd^{2+} and its imaging in living cells. *Inorg. Chim. Acta* **2018**, *482*, 122–129. [CrossRef]

26. Luo, W.; Lei, M.; Wang, Y.; Gao, H.; Wang, Y.; Zhou, Q.; Xu, Z.; Yang, F. An indole–rhodamine-based ratiometric fluorescent probe for Pd^{2+} determination and cell imaging. *Anal. Methods* **2019**, *11*, 1080–1086. [CrossRef]

27. Hu, L.; Lin, Y.; Wang, P.; Zhang, H.; Liu, M.; Mo, S. A rhodamine derivative probe for highly selective detection of Cu(II). *Front. Biosci.* **2022**, *27*, 28. [CrossRef]

28. Qiu, X.; Huang, J.; Wang, N.; Zhao, K.; Cui, J.; Hao, J. Facile Synthesis of Water-Soluble Rhodamine-Based Polymeric Chemosensors via Schiff Base Reaction for Fe($3+$) Detection and Living Cell Imaging. *Front. Chem.* **2022**, *10*, 845627. [CrossRef]

29. Cuc, T.T.K.; Nhien, P.Q.; Khang, T.M.; Chen, H.-Y.; Wu, C.-H.; Hue, B.T.B.; Li, Y.-K.; Wu, J.I.; Lin, H.-C. Controllable FRET processes towards ratiometric Fe3+ ion sensor of pseudo [3] rotaxane containing naphthalimide-based macrocyclic host donor and multi-stimuli responsive rhodamine-modified guest acceptor. *Dye. Pigment.* **2022**, *197*, 109907. [CrossRef]

30. Lee, M.H.; Kim, J.S.; Sessler, J.L. Small molecule-based ratiometric fluorescence probes for cations, anions, and biomolecules. *Chem. Soc. Rev.* **2015**, *44*, 4185–4191. [CrossRef]

31. Williams, D.R. Metals, ligands, and cancer. *Chem. Rev.* **1972**, *72*, 203–213. [CrossRef]

32. Cheng, Z.; Zheng, L.; Xu, H.; Pang, L.; He, H. A rhodamine-based fluorescent probe for Fe3+: Synthesis, theoretical calculation and bioimaging application. *Anal. Methods* **2019**, *11*, 2565–2570. [CrossRef]

33. Min, K.S.; Manivannan, R.; Son, Y.-A. Rhodamine-fluorene based dual channel probe for the detection of Hg2+ ions and its application in digital printing. *Sens. Actuators B Chem.* **2018**, *261*, 545–552. [CrossRef]

34. Hong, M.; Chen, Y.; Zhang, Y.; Xu, D. A novel rhodamine-based Hg2+ sensor with a simple structure and fine performance. *Analist* **2019**, *144*, 7351–7358. [CrossRef] [PubMed]

35. Cicekbilek, F.; Yilmaz, B.; Bayrakci, M.; Gezici, O. An Application of a Schiff-Base Type Reaction in the Synthesis of a New Rhodamine-Based Hg(II)-Sensing Agent. *J. Fluoresc.* **2019**, *29*, 1349–1358. [CrossRef] [PubMed]

36. Patil, S.K.; Das, D. A nanomolar detection of mercury(II) ion by a chemodosimetric rhodamine-based sensor in an aqueous medium: Potential applications in real water samples and as paper strips. *Spectrochim. Acta Part A Mol. Biomol. Spectrosc.* **2019**, *210*, 44–51. [CrossRef]

37. Kan, C.; Shao, X.; Song, F.; Xu, J.; Zhu, J.; Du, L. Bioimaging of a fluorescence rhodamine-based probe for reversible detection of Hg (II) and its application in real water environment. *Microchem. J.* **2019**, *150*, 104142. [CrossRef]

38. Dewangan, S.; Barik, T.; Mishra, S.; Mawatwal, S.; Kumari, S.; Giri, S.; Das, S.; Dhiman, R.; Wölper, C.; Chatterjee, S. Half sandwich based rhodamine-hydrazone single molecule probe: Light responsive, metal sensing and imaging properties. *Appl. Organomet. Chem.* **2018**, *32*, e4612. [CrossRef]

39. Wang, Q.; Jin, L.; Wang, W.; Hu, T.; Chen, C. Rhodamine derivatives as selective "naked-eye" colorimetric and fluorescence off-on sensor for Hg^{2+} in aqueous solution and its applications in bioimaging. *J. Lumin.* **2019**, *209*, 411–419. [CrossRef]

40. Dewangan, S.; Barik, T.; Parida, R.; Mawatwal, S.; Dhiman, R.; Giri, S.; Chatterjee, S. Solvent free synthesis of ferrocene based rhodamine–hydrazone molecular probe with improved bioaccumulation for sensing and imaging applications. *J. Organomet. Chem.* **2019**, *904*, 120999. [CrossRef]

41. Gauthama, B.U.; Narayana, B.; Sarojini, B.K.; Suresh, N.K.; Sangappa, Y.; Kudva, A.K.; Satyanarayana, G.; Raghu, S.V. Colorimetric "off–on" fluorescent probe for selective detection of toxic Hg^{2+} based on rhodamine and its application for in-vivo bioimaging. *Microchem. J.* **2021**, *166*, 106233. [CrossRef]

42. Singh, S.; Coulomb, B.; Boudenne, J.L.; Bonne, D.; Dumur, F.; Simon, B.; Robert-Peillard, F. Sub-ppb mercury detection in real environmental samples with an improved rhodamine-based detection system. *Talanta* **2021**, *224*, 121909. [CrossRef] [PubMed]

43. Li, X.; Li, X.; Zhao, H.; Kang, H.; Fan, C.; Liu, G.; Pu, S. A Novel Diarylethene-rhodamine Unit Based Chemosensor for Fluorimetric and Colorimetric Detection of Hg(2). *J. Fluoresc.* **2021**, *31*, 1513–1523. [CrossRef] [PubMed]

44. Yilmaz, B.; Keskinates, M.; Bayrakci, M. Novel integrated sensing system of calixarene and rhodamine molecules for selective colorimetric and fluorometric detection of Hg$^{(2+)}$ ions in living cells. *Spectrochim. Acta A Mol. Biomol. Spectrosc.* **2021**, *245*, 118904. [CrossRef] [PubMed]

45. Aduroja, O.; Shaw, R.; Abebe, F. A bis(rhodamine 6G)-based fluorescent sensor for Hg^{2+}: Microwave-assisted synthesis, photophysical properties, and computational studies. *Res. Chem. Intermed.* **2022**, *48*, 1847–1861. [CrossRef]

46. Li, M.; Zhang, S.; Zhang, P.; Qin, K.; Xu, B.; Zhou, J.; Yuan, C.; Cao, Q.; Xiao, H. Rhodamine functionalized cellulose for mercury detection and removal: A strategy for providing in situ fluorimetric and colorimetric responses. *Chem. Eng. J.* **2022**, *436*, 135251. [CrossRef]

47. Liang, F.; Xu, L.; Jin, D.; Dong, L.; Lin, S.; Huang, R.; Song, D.; Ma, P. A novel near-infrared fluorescence probe for detecting and imaging Hg$^{(2+)}$ in living cells. *Luminescence* **2022**, *37*, 161–169. [CrossRef]

48. Zhang, Q.; Ding, H.; Xu, X.; Wang, H.; Liu, G.; Pu, S. Rational design of a FRET-based ratiometric fluorescent probe with large Pseudo-Stokes shift for detecting Hg$^{(2+)}$ in living cells based on rhodamine and anthracene fluorophores. *Spectrochim. Acta A Mol. Biomol. Spectrosc.* **2022**, *276*, 121242. [CrossRef]

49. Tromp, A.; De Klerk, C. Effect of copperoxychloride on the fermentation of must and on wine quality. *S. Afr. J. Enol. Vitic.* **1988**, *9*, 31–36. [CrossRef]

50. Doumani, N.; Bou-Maroun, E.; Maalouly, J.; Tueni, M.; Dubois, A.; Bernhard, C.; Denat, F.; Cayot, P.; Sok, N. A New pH-Dependent Macrocyclic Rhodamine B-Based Fluorescent Probe for Copper Detection in White Wine. *Sensors* **2019**, *19*, 4514. [CrossRef]

51. Deepa, A.; Srinivasadesikan, V.; Lee, S.-L.; Padmini, V. Highly Selective and Sensitive Colorimetric and Fluorimetric Sensor for Cu^{2+}. *J. Fluoresc.* **2019**, *30*, 3–10. [CrossRef]

52. Hosseinjani-Pirdehi, H.; Allah Mahmoodi, N.O.; Taheri, A.; Asalemi, K.A.A.; Esmaeili, R. Selective immediate detection of Cu2+ by a pH-sensitive rhodamine-based fluorescence probe in breast cancer cell-line. *Spectrochim. Acta Part A Mol. Biomol. Spectrosc.* **2020**, *229*, 117989. [CrossRef] [PubMed]

53. Karakuş, E. A rhodamine based fluorescent chemodosimeter for the selective and sensitive detection of copper (II) ions in aqueous media and living cells. *J. Mol. Struct.* **2021**, *1224*, 129037. [CrossRef]

54. Wang, Y.; Wang, Y.; Guo, F.; Wang, Y.; Xie, P. A new naked-eye fluorescent chemosensor for Cu(II) and its practical applications. *Res. Chem. Intermed.* **2021**, *47*, 3515–3528. [CrossRef]

55. Yang, L.; Zhang, X.; Yang, J.; Yuan, M.-S.; Wang, J. A rhodamine-based chemosensor and functionalized gel ball for detecting and adsorbing copper ions. *Tetrahedron* **2021**, *80*, 131893. [CrossRef]

56. Liu, Y.; Zhao, C.; Zhao, X.; Liu, H.; Wang, Y.; Du, Y.; Wei, D. A selective N,N-dithenoyl-rhodamine based fluorescent probe for Fe^{3+} detection in aqueous and living cells. *J. Environ. Sci.* **2020**, *90*, 180–188. [CrossRef]

57. Wang, K.-P.; Zheng, W.-J.; Lei, Y.; Zhang, S.-J.; Zhang, Q.; Chen, S.; Hu, Z.-Q. A thiophene-rhodamine dyad as fluorescence probe for ferric ion and its application in living cells imaging. *J. Lumin.* **2019**, *208*, 468–474. [CrossRef]

58. Wang, Y.; Guo, R.; Hou, X.; Lei, M.; Zhou, Q.; Xu, Z. Highly Sensitive and Selective Fluorescent Probe for Detection of Fe^{3+} Based on Rhodamine Fluorophore. *J. Fluoresc.* **2019**, *29*, 645–652. [CrossRef] [PubMed]

59. Zhang, M.; Shen, C.; Jia, T.; Qiu, J.; Zhu, H.; Gao, Y. One-step synthesis of rhodamine-based Fe3+ fluorescent probes via Mannich reaction and its application in living cell imaging. *Spectrochim. Acta Part A Mol. Biomol. Spectrosc.* **2020**, *231*, 118105. [CrossRef]

60. Chen, Y.; Wu, Y.; Zhu, Y.; Tian, S. A fluorescent polyurethane foam based on rhodamine derivative as Fe(III) sensor in pure water. *Polym. Int.* **2021**, *71*, 169–174. [CrossRef]

61. Liu, X.; Chen, Z.; Gao, R.; Kan, C.; Xu, J. Portable quantitative detection of Fe^{3+} by integrating a smartphone with colorimetric responses of a rhodamine-functionalized polyacrylamide hydrogel chemosensor. *Sens. Actuators B Chem.* **2021**, *340*, 129958. [CrossRef]

62. Qin, Z.; Su, W.; Liu, P.; Ma, J.; Zhang, Y.; Jiao, T. Facile Preparation of a Rhodamine B Derivative-Based Fluorescent Probe for Visual Detection of Iron Ions. *ACS Omega* **2021**, *6*, 25040–25048. [CrossRef] [PubMed]

63. Zhang, J.; Bai, C.B.; Chen, M.Y.; Yue, S.Y.; Qin, Y.X.; Liu, X.Y.; Xu, M.Y.; Zheng, Q.J.; Zhang, L.; Li, R.Q.; et al. Novel Fluorescent Probe toward Fe$^{(3+)}$ Based on Rhodamine 6G Derivatives and Its Bioimaging in Adult Mice, Caenorhabditis elegans, and Plant Tissues. *ACS Omega* **2021**, *6*, 8616–8624. [CrossRef] [PubMed]

64. Liu, X.; Chen, Z.; Gao, R.; Kan, C.; Xu, J. A paper-based fluorescent and colorimetric portable device with smartphone application for Fe^{3+} sensing. *J. Environ. Chem. Eng.* **2022**, *10*, 107650. [CrossRef]

65. Xie, X.; Pan, M.; Hong, L.; Liu, K.; Yang, J.; Wang, S.; Wang, S. An "Off-On" Rhodamine 6G Hydrazide-Based Output Platform for Fluorescence and Visual Dual-Mode Detection of Lead(II). *J. Agric. Food Chem.* **2021**, *69*, 7209–7217. [CrossRef]

66. Karmegam, M.V.; Karuppannan, S.; Christopher Leslee, D.B.; Subramanian, S.; Gandhi, S. Phenothiazine–rhodamine-based colorimetric and fluorogenic 'turn-on' sensor for Zn^{2+} and bioimaging studies in live cells. *Luminescence* **2019**, *35*, 90–97. [CrossRef]

67. Zhang, X.; Jin, G.; Chen, Z.; Wu, Y.; Li, Q.; Liu, P.; Xi, G. An efficient turn-on fluorescence chemosensor system for Zn(II) ions detection and imaging in mitochondria. *J. Photochem. Photobiol. B* **2022**, *234*, 112485. [CrossRef] [PubMed]

68. Paul, S.; Bhuyan, S.; Mukhopadhyay, S.K.; Murmu, N.C.; Banerjee, P. Sensitive and Selective in Vitro Recognition of Biologically Toxic As(III) by Rhodamine Based Chemoreceptor. *ACS Sustain. Chem. Eng.* **2019**, *7*, 13687–13697. [CrossRef]

69. Kan, C.; Wu, L.; Wang, X.; Shao, X.; Qiu, S.; Zhu, J. Rhodamine B-based chemiluminescence sensor for aluminum ion monitoring and bioimaging applications. *Tetrahedron* **2021**, *85*, 132054. [CrossRef]

70. Jiang, T.; Bian, W.; Kan, J.; Sun, Y.; Ding, N.; Li, W.; Zhou, J. Sensitive and rapid detection of Cr(3+) in live cells by a red turn-on fluorescent probe. *Spectrochim. Acta A Mol. Biomol. Spectrosc.* **2021**, *245*, 118903. [CrossRef]

71. Rathinam, B.; Murugesan, V.; Liu, B.-T. Fluorescent "OFF–ON" Sensors for the Detection of Sn^{2+} Ions Based on Amine-Functionalized Rhodamine 6G. *Chemosensors* **2022**, *10*, 69. [CrossRef]

72. Fukuda, T.; Ewan, L.; Bauer, M.; Mattaliano, R.J.; Zaal, K.; Ralston, E.; Plotz, P.H.; Raben, N. Dysfunction of endocytic and autophagic pathways in a lysosomal storage disease. *Ann. Neurol. Off. J. Am. Neurol. Assoc. Child Neurol. Soc.* **2006**, *59*, 700–708. [CrossRef] [PubMed]

73. Yu, M.; Wu, X.; Lin, B.; Han, J.; Yang, L.; Han, S. Lysosomal pH decrease in inflammatory cells used to enable activatable imaging of inflammation with a sialic acid conjugated profluorophore. *Anal. Chem.* **2015**, *87*, 6688–6695. [CrossRef] [PubMed]

74. Webb, B.A.; Chimenti, M.; Jacobson, M.P.; Barber, D.L. Dysregulated pH: A perfect storm for cancer progression. *Nat. Rev. Cancer* **2011**, *11*, 671–677. [CrossRef] [PubMed]

75. Mao, G.-J.; Liang, Z.-Z.; Gao, G.-Q.; Wang, Y.-Y.; Guo, X.-Y.; Su, L.; Zhang, H.; Ma, Q.-J.; Zhang, G. A photostable Si-rhodamine-based near-infrared fluorescent probe for monitoring lysosomal pH during heat stroke. *Anal. Chim. Acta* **2019**, *1092*, 117–125. [CrossRef]

76. Lee, D.; Swamy, K.M.K.; Hong, J.; Lee, S.; Yoon, J. A rhodamine-based fluorescent probe for the detection of lysosomal pH changes in living cells. *Sens. Actuators B Chem.* **2018**, *266*, 416–421. [CrossRef]

77. Urano, Y.; Asanuma, D.; Hama, Y.; Koyama, Y.; Barrett, T.; Kamiya, M.; Nagano, T.; Watanabe, T.; Hasegawa, A.; Choyke, P.L. Selective molecular imaging of viable cancer cells with pH-activatable fluorescence probes. *Nat. Med.* **2009**, *15*, 104. [CrossRef]

78. Koide, Y.; Kojima, R.; Hanaoka, K.; Numasawa, K.; Komatsu, T.; Nagano, T.; Kobayashi, H.; Urano, Y. Design strategy for germanium-rhodamine based pH-activatable near-infrared fluorescence probes suitable for biological applications. *Commun. Chem.* **2019**, *2*, 94. [CrossRef]

79. Wang, J.; Xia, S.; Bi, J.; Zhang, Y.; Fang, M.; Luck, R.L.; Zeng, Y.; Chen, T.-H.; Lee, H.-M.; Liu, H. Near-infrared fluorescent probes based on TBET and FRET rhodamine acceptors with different pKa values for sensitive ratiometric visualization of pH changes in live cells. *J. Mater. Chem. B* **2019**, *7*, 198–209. [CrossRef]

80. Yan, Y.; Zhang, X.; Zhang, X.; Li, N.; Man, H.; Chen, L.; Xiao, Y. Ratiometric sensing lysosomal pH in inflammatory macrophages by a BODIPY-rhodamine dyad with restrained FRET. *Chin. Chem. Lett.* **2019**, *31*, 1091–1094. [CrossRef]

81. Liu, Z.; Wang, L.; Zhu, W.; Ding, Y.; Liu, S.; Wang, Q.; Chen, Y. A versatile color and fluorescence pH sensor based on AIE and open-loop synergy effect: Crystal structure and its application in cell imaging. *Dye. Pigment.* **2021**, *190*, 109310. [CrossRef]

82. Srivastava, P.; Fürstenwerth, P.C.; Witte, J.F.; Resch-Genger, U. Synthesis and spectroscopic characterization of a fluorescent phenanthrene-rhodamine dyad for ratiometric measurements of acid pH values. *New J. Chem.* **2021**, *45*, 13755–13762. [CrossRef]

83. Kimura, H. Hydrogen sulfide: Its production, release and functions. *Amino Acids* **2011**, *41*, 113–121. [CrossRef] [PubMed]

84. Blackstone, E.; Morrison, M.; Roth, M.B. H_2S induces a suspended animation–like state in mice. *Science* **2005**, *308*, 518. [CrossRef] [PubMed]

85. Xu, F.; Gao, X.; Li, H.; Xu, S.; Li, X.; Hu, X.; Li, Z.; Xu, J.; Hua, H.; Li, D. Hydrogen sulfide releasing enmein-type diterpenoid derivatives as apoptosis inducers through mitochondria-related pathways. *Bioorganic Chem.* **2019**, *82*, 192–203. [CrossRef]

86. Hu, X.; Jiao, R.; Li, H.; Wang, X.; Lyu, H.; Gao, X.; Xu, F.; Li, Z.; Hua, H.; Li, D. Antiproliferative hydrogen sulfide releasing evodiamine derivatives and their apoptosis inducing properties. *Eur. J. Med. Chem.* **2018**, *151*, 376–388. [CrossRef]

87. Gadalla, M.M.; Snyder, S.H. Hydrogen sulfide as a gasotransmitter. *J. Neurochem.* **2010**, *113*, 14–26. [CrossRef]

88. de Mel, A.; Murad, F.; Seifalian, A.M. Nitric oxide: A guardian for vascular grafts? *Chem. Rev.* **2011**, *111*, 5742–5767. [CrossRef]

89. Pacher, P.; Beckman, J.S.; Liaudet, L. Nitric oxide and peroxynitrite in health and disease. *Physiol. Rev.* **2007**, *87*, 315–424. [CrossRef]

90. Wang, Q.; Jiao, X.; Liu, C.; He, S.; Zhao, L.; Zeng, X. A rhodamine-based fast and selective fluorescent probe for monitoring exogenous and endogenous nitric oxide in live cells. *J. Mater. Chem. B* **2018**, *6*, 4096–4103. [CrossRef]

91. Alam, R.; Islam, A.S.M.; Sasmal, M.; Katarkar, A.; Ali, M. A rhodamine-based turn-on nitric oxide sensor in aqueous medium with endogenous cell imaging: An unusual formation of nitrosohydroxylamine. *Org. Biomol. Chem.* **2018**, *16*, 3910–3920. [CrossRef]

92. Podder, A.; Koo, S.; Lee, J.; Mun, S.; Khatun, S.; Kang, H.-G.; Bhuniya, S.; Kim, J.S. A rhodamine based fluorescent probe validates substrate and cellular hypoxia specific NADH expression. *Chem. Commun.* **2019**, *55*, 537–540. [CrossRef] [PubMed]

93. Gu, T.; Mo, S.; Mu, Y.; Huang, X.; Hu, L. Detection of endogenous hydrogen peroxide in living cells with para-nitrophenyl oxoacetyl rhodamine as turn-on mitochondria-targeted fluorescent probe. *Sens. Actuators B Chem.* **2020**, *309*, 127731. [CrossRef]

94. Liu, Y.; Lee, D.; Wu, D.; Swamy, K.M.K.; Yoon, J. A new kind of rhodamine-based fluorescence turn-on probe for monitoring ATP in mitochondria. *Sens. Actuators B Chem.* **2018**, *265*, 429–434. [CrossRef]

95. Tikum, A.F.; Kim, G.; Nasirian, A.; Ko, J.W.; Yoon, J.; Kim, J. Rhodamine-based near-infrared probe for emission detection of ATP in lysosomes in living cells. *Sens. Actuators B Chem.* **2019**, *292*, 40–47. [CrossRef]

96. Ran, F.; Ma, C.; Xiang, Y.; Xu, Y.; Liu, X.; Zhang, H. A fluorescent and colorimetric dual-channel sensor based on acid phosphatase-triggered blocking of internal filtration effect. *Mikrochim. Acta* **2021**, *188*, 282. [CrossRef]

97. Tang, J.; Li, Q.; Guo, Z.; Zhu, W. A fast-response and highly specific Si-Rhodamine probe for endogenous peroxynitrite detection in living cells. *Org. Biomol. Chem.* **2019**, *17*, 1875–1880. [CrossRef]

98. Wu, J.; Ye, Z.; Wu, F.; Wang, H.; Zeng, L.; Bao, G.-M. A rhodamine-based fluorescent probe for colorimetric and fluorescence lighting-up determination of toxic thiophenols in environmental water and living cells. *Talanta* **2018**, *181*, 239–247. [CrossRef]

99. Wang, Z.; Zhang, Q.; Liu, J.; Sui, R.; Li, Y.; Li, Y.; Zhang, X.; Yu, H.; Jing, K.; Zhang, M.; et al. A twist six-membered rhodamine-based fluorescent probe for hypochlorite detection in water and lysosomes of living cells. *Anal. Chim. Acta* **2019**, *1082*, 116–125. [CrossRef]

100. Zhang, D.; Ma, Z.; Wang, Y.; Yin, H.; Li, M.; Wang, Y.; Wang, H.; Jia, B.; Liu, J. Dual-binding benzene and rhodamine B conjugate derivatives as fluorescent chemodosimeter for hypochlorite in living cell imaging. *Spectrochim. Acta Part A Mol. Biomol. Spectrosc.* **2020**, *229*, 117908. [CrossRef]

101. Wang, K.; Wang, W.; Chen, S.-Y.; Guo, J.-C.; Li, J.-H.; Yang, Y.-S.; Wang, X.-M.; Xu, C.; Zhu, H.-L. A novel Near-Infrared rhodamine-derivated turn-on fluorescence probe for sensing SO_3^{2-} detection and their bio-imaging in vitro and in vivo. *Dye. Pigment.* **2021**, *188*, 109229. [CrossRef]

102. Shang, H.; Chen, H.; Tang, Y.; Ma, Y.; Lin, W. Development of a two-photon fluorescent turn-on probe with far-red emission for thiophenols and its bioimaging application in living tissues. *Biosens. Bioelectron.* **2017**, *95*, 81–86. [CrossRef] [PubMed]

103. Khandare, D.G.; Banerjee, M.; Gupta, R.; Kumar, N.; Ganguly, A.; Singh, D.; Chatterjee, A. Green synthesis of a benzothiazole based 'turn-on'type fluorimetric probe and its use for the selective detection of thiophenols in environmental samples and living cells. *RSC Adv.* **2016**, *6*, 52790–52797. [CrossRef]

104. Stanford, B.D.; Pisarenko, A.N.; Snyder, S.A.; Gordon, G. Perchlorate, bromate, and chlorate in hypochlorite solutions: Guidelines for utilities. *J. -Am. Water Work. Assoc.* **2011**, *103*, 71–83. [CrossRef]

105. Bruch, M.K. Toxicity and safety of topical sodium hypochlorite. In *Disinfection by Sodium Hypochlorite: Dialysis Applications*; Karger Publishers: Berlin, Germany, 2007; Volume 154, pp. 24–38.

106. Chang, L.L.; Gao, Q.; Liu, S.; Hu, C.C.; Zhou, W.J.; Zheng, M.M. Selective and differential detection of Hg^{2+} and Cu^{2+} with use of a single rhodamine hydrazone-type probe in the absence and presence of UV irradiation. *Dye. Pigment.* **2018**, *153*, 117–124. [CrossRef]

107. Wang, K.; Kong, Q.; Chen, X.; Yoon, J.; Swamy, K.M.K.; Wang, F. A bifunctional rhodamine derivative as chemosensor for recognizing Cu^{2+} and Hg^{2+} ions via different spectra. *Chin. Chem. Lett.* **2019**, *31*, 1087–1090. [CrossRef]

108. Ozmen, P.; Demir, Z.; Karagoz, B. An easy way to prepare reusable rhodamine-based chemosensor for selective detection of Cu^{2+} and Hg^{2+} ions. *Eur. Polym. J.* **2022**, *162*, 110922. [CrossRef]

109. Mondal, S.; Bandyopadhyay, C.; Ghosh, K. Chromenone-rhodamine conjugate for naked eye detection of Al^{3+} and Hg^{2+} ions in semi aqueous medium. *Supramol. Chem.* **2018**, *31*, 1–8. [CrossRef]

110. Erdemir, S. Fluorometric dual sensing of Hg^{2+} and Al^{3+} by novel triphenylamine appended rhodamine derivative in aqueous media. *Sens. Actuators B Chem.* **2019**, *290*, 558–564. [CrossRef]

111. Hazra, A.; Ghosh, P.; Roy, P. A rhodamine based dual chemosensor for $Al(^{3+})$ and $Hg(^{2+})$: Application in the construction of advanced logic gates. *Spectrochim. Acta A Mol. Biomol. Spectrosc.* **2022**, *271*, 120905. [CrossRef]

112. Chan, W.C.; Saad, H.M.; Sim, K.S.; Lee, V.S.; Tan, K.W. A rapid turn-on dual functional rhodamine B probe for aluminum (III) and copper (II) that can be utilised as a molecular logic gate and in water analysis. *J. Mol. Struct.* **2022**, *1254*, 132337. [CrossRef]

113. Zhang, Z.; Deng, C.; Song, H. A novel rhodamine-based turn-on fluorescent probe for dual detection of Cr^{3+} and Cu^{2+} with solvent-dependent binding properties. *Inorg. Chem. Commun.* **2018**, *95*, 56–60. [CrossRef]

114. Mehta, R.; Kaur, P.; Choudhury, D.; Paul, K.; Luxami, V. Al^{3+} induced hydrolysis of rhodamine-based Schiff-base: Applications in cell imaging and ensemble as CN-sensor in 100% aqueous medium. *J. Photochem. Photobiol. A Chem.* **2019**, *380*, 111851. [CrossRef]

115. Zhu, L.; Liao, W.; Chang, H.; Liu, X.; Miao, S. A Novel Fluorescent Probe for Detection of Hydrogen Sulfide and Its Bioimaging Applications in Living Cells. *ChemistrySelect* **2020**, *5*, 829–833. [CrossRef]

116. Das, D.; Alam, R.; Katarkar, A.; Ali, M. A differentially selective probe for trivalent chemosensor upon single excitation with cell imaging application: Potential applications in combinatorial logic circuit and memory devices. *Photochem. Photobiol. Sci.* **2019**, *18*, 242–252. [CrossRef] [PubMed]

117. Singha, D.; Das, T.; Satyanarayana, L.; Roy, P.; Nandi, M. Rhodamine functionalized mesoporous silica as a chemosensor for the efficient sensing of Al^{3+}, Cr^{3+} and Fe^{3+} ions and their removal from aqueous media. *New J. Chem.* **2019**, *43*, 15563–15574. [CrossRef]

118. Roy, A.; Das, S.; Sacher, S.; Mandal, S.K.; Roy, P. A rhodamine based biocompatible chemosensor for Al^{3+}, Cr^{3+} and Fe^{3+} ions: Extraordinary fluorescence enhancement and a precursor for future chemosensors. *Dalton Trans.* **2019**, *48*, 17594–17604. [CrossRef]

119. Banerjee, M.; Ghosh, M.; Ta, S.; Das, J.; Das, D. A smart optical probe for detection and discrimination of Zn^{2+}, Cd^{2+} and Hg^{2+} at nano-molar level in real samples. *J. Photochem. Photobiol. A Chem.* **2019**, *377*, 286–297. [CrossRef]

120. Sadak, A.E.; Karakuş, E. Triazatruxene–Rhodamine-Based Ratiometric Fluorescent Chemosensor for the Sensitive, Rapid Detection of Trivalent Metal Ions: Aluminium (III), Iron (III) and Chromium (III). *J. Fluoresc.* **2020**, *30*, 213–220. [CrossRef]

121. Wang, Y.; Wu, H.; Wu, W.N.; Mao, X.J.; Zhao, X.L.; Xu, Z.Q.; Xu, Z.H.; Fan, Y.C. Novel rhodamine-based colorimetric and fluorescent sensor for the dual-channel detection of $Cu(^{2+})$ and $Co(^{2+})$/trivalent metal ions and its AIRE activities. *Spectrochim. Acta A Mol. Biomol. Spectrosc.* **2019**, *212*, 1–9. [CrossRef]

122. Pungut, N.A.S.; Heng, M.P.; Saad, H.M.; Sim, K.S.; Lee, V.S.; Tan, K.W. From one to three, modifications of sensing behavior with solvent system: DFT calculations and real-life application in detection of multianalytes (Cu^{2+}, Ni^{2+} and Co^{2+}) based on a colorimetric Schiff base probe. *J. Mol. Struct.* **2021**, *1238*, 130453. [CrossRef]

123. Hazra, A.; Roy, P. A rhodamine based dye for sensing of Group 13 metal ions. *Anal. Chim. Acta* **2022**, *1193*, 339378. [CrossRef] [PubMed]

124. Podshibyakin, V.A.; Shepelenko, E.N.; Karlutova, O.Y.; Dubonosova, I.V.; Borodkin, G.S.; Popova, O.S.; Zaichenko, S.B.; Dubonosov, A.D.; Bren, V.A.; Minkin, V.I. Solvent-dependent selective "naked eye" chromofluorogenic multifunctional rhodamine-based probe for Al^{3+}, Cu^{2+}, Hg^{2+}, S^{2-} and CN^{-} ions. *Tetrahedron* **2022**, *110*, 132710. [CrossRef]
125. Kilic, H.; Bozkurt, E. A rhodamine-based novel turn on trivalent ions sensor. *J. Photochem. Photobiol. A Chem.* **2018**, *363*, 23–30. [CrossRef]